HHS Public Access

Author manuscript

Curr Biol. Author manuscript; available in PMC 2022 October 25.

Published in final edited form as:

Curr Biol. 2021 October 25; 31(20): 4499–4511.e8. doi:10.1016/j.cub.2021.08.004.

The what and when of olfactory working memory in humans

Andrew I Yang[1,*], **Gulce N Dikecligil**[2], **Heidi Jiang**[3], **Sandhitsu R Das**[4], **Joel M Stein**[4], **Stephan U Schuele**[3], **Joshua M Rosenow**[5], **Kathryn A Davis**[6], **Timothy H Lucas**[1], **Jay A Gottfried**[2,6]

[1]Department of Neurosurgery, Perelman School of Medicine, University of Pennsylvania, Philadelphia, PA, 19104, USA

[2]Department of Psychology, School of Arts and Sciences, University of Pennsylvania, Philadelphia, PA, 19104, USA

[3]Department of Neurology, Feinberg School of Medicine, Northwestern University, Chicago, IL, 60611, USA

[4]Department of Radiology, Perelman School of Medicine, University of Pennsylvania, Philadelphia, PA, 19104, USA

[5]Department of Neurosurgery, Feinberg School of Medicine, Northwestern University, Chicago, IL, 60611, USA

[6]Department of Neurology, Perelman School of Medicine, University of Pennsylvania, Philadelphia, PA, 19104, USA

Abstract

Encoding and retaining novel sequences of sensory stimuli in working memory is crucial for adaptive behavior. A fundamental challenge for the central nervous system is to maintain each sequence item in an active and discriminable state, while also preserving their temporal context. Nested neural oscillations have been postulated to disambiguate the “what” and “when” of sequences, but the mechanisms by which these multiple streams of information are coordinated in the human brain remain unclear. Drawing from foundational animal studies[1,2], we recorded local field potentials from the human piriform cortex and hippocampus during a working memory

Correspondence: Andrew I. Yang, MD, MS, Department of Neurosurgery, Perelman School of Medicine, University of Pennsylvania, Philadelphia, PA 19104, iyang.and@gmail.com; Jay A. Gottfried, MD, PhD, Arthur H. Rubenstein University Professor, Penn Integrates Knowledge University Professor, Department of Neurology, Psychology, Perelman School of Medicine, University of Pennsylvania, Philadelphia, PA 19104, jaygottf@pennmedicine.upenn.edu.

*Lead Contact

Author Contributions: Conceptualization, A.I.Y., H.J., J.A.G.; Methodology, A.I.Y., G.N.D., H.J.; Software, A.I.Y., G.N.D., H.J., S.R.D., J.M.S.; Formal Analysis A.I.Y.; Investigation A.I.Y., G.N.D., H.J., S.U.S., J.M.R., K.A.D., T.H.L.; Resources S.U.S., J.M.R., K.A.D., T.H.L., J.A.G.; Writing – Original Draft A.I.Y., J.A.G.; Writing – Review & Editing A.I.Y., G.N.D., J.A.G.; Visualization A.I.Y., G.N.D.; Supervision J.A.G.

Declaration of Interests: The authors declare no competing interests.

Inclusion and Diversity Statement: We worked to ensure that the study questionnaires were prepared in an inclusive way. While citing references scientifically relevant for this work, we also actively worked to promote gender balance in our reference list.

task in which subjects experienced sequences of three distinct odors. Our data revealed a unique organization of odor memories across multiple timescales of the theta rhythm. During encoding, odors elicited greater gamma at distinct theta phases in both regions, time-stamping their positions in the sequence, whereby the robustness of this effect was predictive of temporal order memory. During maintenance, stimulus-driven patterns of theta-coupled gamma were spontaneously reinstated in piriform cortex, recapitulating the order of the initial sequence. Replay events were time-compressed across contiguous theta cycles, coinciding with periods of enhanced piriform-hippocampal theta phase synchrony, and their prevalence forecasted subsequent recall accuracy on a trial-by-trial basis. Our data provide a novel link between endogenous replay orchestrated by the theta rhythm and short-term retention of sequential memories in the human brain.

Keywords

electrocorticography; ECoG; intracranial electroencephalography; intracranial EEG; epilepsy; local field potential; neural oscillations; theta; gamma; phase amplitude coupling; PAC; nested oscillations; phase coding; temporal multiplexing; working memory; sequence memory; replay; hippocampus; odor perception; olfactory system; piriform cortex

INTRODUCTION

In the natural world, animals make use of a complex stream of olfactory inputs to guide essential behavior. For example, dogs can determine the direction of an odor trail based on information acquired from sequential sampling of multiple footsteps[3]. As another example, insects are able to localize the source of turbulent odor plumes in spite of the absence of concentration gradients, with flight patterns reflecting reactive odor responses as well as their modulation based on the history of odor encounters on the timescale of seconds.[3,4] Such behavior suggests that encoded temporal sequences of sensory stimuli are being maintained in working memory. Indeed, rodents can remember the temporal order of once-presented sequences of distinct odors[1,2]. Together, these observations underscore the ethological relevance of encoding both the content and temporal structure inherent in a novel sequence of odor stimuli.

Similarly, behavioral studies have established that humans can encode and maintain a sequence of odors in working memory[5]. However, a general challenge for ensuring the fidelity of a sequence is the fact that individual items may draw from shared cognitive resources in the same brain regions, giving rise to potential neural and perceptual misattributions[6,7]. In fact, distinct odors evoke distributed and highly overlapping patterns of population activity in the piriform cortex (PCx)[8]. In addition, without a mechanism to timestamp when each smell was encountered, sequence-related ordinal information becomes inaccessible. This dilemma of maintaining both the content and the temporal context of an odor sequence represents the “what” and “when” questions of olfactory sequence memory.

Neural oscillations have been hypothesized to disambiguate and sustain sequence representations[9–12]. Specifically, an influential theoretical framework[13–17] focused on theta-nested gamma oscillations[18–21] has generated two predictions about the oscillatory

mechanisms underlying sequence memory. First, interference between individual memory items is minimized by temporally segregating stimulus-specific gamma activity[12,21–25] within distinct phases of a theta cycle, or across separate theta cycles. Second, items are retained via the sequential reactivation of each memory trace, with replay of the entire sequence temporally compressed into theta timescales to allow multiple items to be maintained in working memory. Whereas the rodent hippocampus literature has provided evidence for coordination of spatial (environment) memory representations across multiple theta timescales[26–29], there is limited support for such an organization in human memory.

The olfactory system represents a unique model for elucidating the mechanisms that shape and sustain sequence memory. Foundational work in rodents established that hippocampal lesions induce selective deficits in memory for the temporal context of odors, while sparing memory for individual odors[1,2]. On the other hand, suppression of odor-specific delay activity in the rodent PCx impairs odor object memory[30]. This functional dissociation suggests that these structures must work together to retain the content and context of odor sequences. Anatomically, the PCx and hippocampus are disynaptically linked in the medial temporal lobe[31], and both animal[32] and human[33,34] studies have revealed oscillatory phase synchrony between the PCx and hippocampus during odor sampling, highlighting a potential mode for inter-regional communication[35]. In the current study, we utilized simultaneous local field potential (LFP) recordings from the human PCx and anterior hippocampus (AH) to test the hypothesis that coupled theta and gamma oscillations support mnemonic representations of the “what” and “when” of odor sequences (Figure 1, S1; Table S1).

RESULTS

Behavioral performance

Subjects (N = 8) took part in a novel olfactory variant of the Sternberg three-item working memory task[36](Figure 1A, B). On each trial, subjects smelled a novel sequence of three distinct cue odors (encoding period), randomly selected from a set of ten distinct odor types. After a short delay period of 7–10 seconds (maintenance), subjects were presented with a probe odor (retrieval) and asked whether it had appeared in the sequence (identity match judgment; chance accuracy 50%). If a match was reported, they were then asked whether the odor had appeared in the first, second, or third position (sequence position judgment; chance 33%). All subjects performed well above chance on both probe judgments (Figure 1D, E), with the exception of one subject (black dot) who was retained for analysis given above chance performance on the sequence position judgment.

Coupled oscillations during encoding and maintenance of odor sequences

The conceptual framework of this study is that nested oscillations support the encoding and maintenance of odor sequences. The basic idea is that coupling between the phase of a low-frequency *modulating* oscillation and the magnitude of a high-frequency *modulated* oscillation, i.e., phase-amplitude coupling (PAC), creates a multi-dimensional scaffold for parsing both stimulus content and temporal context. Visual inspection of single trials revealed high-frequency oscillations occurring in the form of temporally brief, narrow-band bursts (Figure 2A), similar to previous observations during olfactory[37,38] or mnemonic

processing[23,39]. To determine whether these bursts had a systematic relationship to the phase of an underlying low-frequency rhythm, we utilized a PAC metric that treats modulated oscillations as discrete events[40]. First, we identified periods of enhanced high-frequency activity (>2 s.d. above mean power during the pre-encoding baseline, obtained from the fixation cross period shown in Figure 1A) that was sustained for more than three cycles. Second, these oscillatory events were used as trigger time points to compute the average, peri-event raw LFP signal (*modulatory signal*), from which we quantified the *modulation strength* as well as the predominant frequency of the modulating oscillation (see analysis schematic in Figure S2). Third, significance was assessed with respect to a surrogate distribution constructed from randomly sampled trigger time points.

In each subject, we evaluated PAC independently for each narrow-band oscillation whose center frequencies tiled a wide range of candidate modulated frequencies (i.e., 20–200 Hz). During encoding and maintenance, we found significant coupling (Bonferroni-corrected across modulated sub-bands, $p < 0.025$) between oscillatory bursts in the 20–100 Hz range and theta (3–8 Hz) phase, in both PCx and AH (Figure 2B). Although 20–100 Hz includes frequencies that have been referred to as high beta or gamma, similar frequency ranges have been reported in past human studies of sequence memory[18,41]. For simplicity, we refer to this range as gamma. Moreover, in line with prior intracranial recordings[41–43], each subject exhibited a diversity in the specific frequencies within the theta and gamma bands that were coupled (see e.g. in Figure S2A). From a theoretical perspective, such diversity is thought to be critical for a physiological substrate capable of representing multiple streams of information[9,12].

To further demonstrate the task-dependent emergence of these nested oscillations, we conducted two additional analyses. First, using data from the power spectra of each task period[44] (see single-subject e.g. in Figure S3A-B), we confirmed that there was a clear theta-band peak in both regions of interest (Figure S3C). Consistent with previous human data[45], theta power during encoding (paired-sample *t*-test; PCx, $t_6 = 2.97$, $p = 0.03$; AH, $t_5 = 2.94$, $p = 0.03$) and maintenance (PCx, $t_6 = 2.46$, $p = 0.049$; AH, $t_5 = 2.86$, $p = 0.035$) were each increased relative to the pre-encoding baseline (Figure 2C). Within subjects, the center frequencies of theta-band peaks were congruent with the modulating frequency at maximal coupling with gamma bursts (Figure S3D).

Second, we assessed for task-dependent changes in the strength of theta-gamma coupling during encoding and maintenance over baseline. To account for the fact that each subject had multiple theta-modulated sub-bands within the gamma frequency range, we combined data from task periods and baseline to identify the specific sub-band (for each subject) associated with the strongest modulation by theta phase (see Methods). In this way, we found that the modulation strengths of theta-coupled gamma bursts during encoding and maintenance were increased compared to during baseline (paired-sample *t*-test; PCx, $t_6 = 5.16$, $p = 0.002$; AH, $t_5 = 7.57$, $p < 0.001$; Figure 2D). Using a similar approach, we found that this task-related upregulation was further stratified based on behavior, with increased theta phase modulation of gamma bursts during identity match-correct vs. incorrect trials (PCx, $t_6 = 4.66$, $p = 0.004$; AH, $t_5 = 5.74$, $p = 0.002$). In contrast, there was no difference in the prevalence of gamma bursts for either of the above two contrasts (paired-sample *t*-test, $p > 0.05$; see Methods).

These results suggest that the strength of modulation of gamma bursts by the underlying theta oscillation, rather than the prevalence of gamma bursts *per se*, is more relevant for encoding and maintenance.

Encoding the "when" of odor sequences

Having established the task-dependent emergence of nested theta and gamma oscillations, we next investigated how these dual oscillations may underlie multiplexed representations of odor sequences during their initial encoding. Mechanistically, theta-gamma PAC opens up the possibility that the occurrence of gamma bursts at distinct phases of theta, could constitute representations of sequence position (i.e., "theta phase coding")[12,42]. We expected to observe theta phase coding in PCx, where it would serve to mitigate interference between cue odors during their sequential encoding[6–8], as well as in AH, given its involvement in mapping the temporal succession of events[10,46,47].

First, we asked whether there was a *consistent* theta phase preference, across trials, for cue odors presented in each of the three sequence positions (independent of odor identity). To test this, for each cue odor trial, we binned stimulus-driven gamma power across theta phase (60 bins spanning [-π, π]) to generate a phase distribution of gamma. We then computed the trial-averaged phase distributions for each sequence position and identified significant phase clusters with respect to time-shuffled surrogate data (cluster-corrected across phase bins, $p < 0.025$). At the single-subject level, we found that odor-induced gamma activity for each sequence position was confined to phase-specific clusters of the theta cycle, in both PCx and AH (Figure 3A). Importantly, this effect was conditional on subsequent temporal order recall. At the group level, the number of sequence positions with significant phase clusters for each subject ([0, 1, 2, or 3]) was greater for sequence position correct vs. incorrect trials (Figure 3B): in PCx, 2.2 ± 0.3 (mean ± s.e.m.) vs. 0.8 ± 0.2 (paired-sample *t*-test, $t_5 = 4.00$, $p = 0.01$); in AH, 2.5 ± 0.2 vs. 0.8 ± 0.4 ($t_5 = 2.71$, $p = 0.04$). Note that subjects had correctly answered the identity match judgment in both subsets of trials, and so the only behavioral difference was performance on the sequence position judgment.

Second, we asked whether preferred theta phases were sufficiently *separable* between the three sequence positions, which would be necessary to serve as robust representations of sequence position. For this analysis, we determined the overall phase preference of each single-trial gamma response to cue odors from the largest cluster of the corresponding theta phase distribution (see Methods). For each subject and region of interest, the separability of preferred theta phases was assessed between each unique pair of sequence positions (i.e., position 1 vs. 2, 2 vs. 3, 1 vs. 3). As in the above phase consistency analysis, the number of significant phase difference tests (Watson-William test, $p < 0.05$) per subject was greater during successful vs. unsuccessful sequence memory formation (Figure 3C): in PCx, 2.2 ± 0.3 vs. 0.3 ± 0.3 (paired-sample *t*-test, $t_5 = 5.97$, $p = 0.002$); in AH, 2.8 ± 0.2 vs. 0.3 ± 0.3 ($t_5 = 7.32$, $p < 0.001$). In sum, we showed that the position-dependent theta phase preference was both *consistent* across trials as well as *separable* in phase space. These data provide compelling evidence that theta phase coding is critical for encoding behaviorally relevant representations of olfactory temporal context, dissociated from odor object coding.

Encoding the "what" of odor sequences

Next, we focused on whether coupled theta and gamma oscillations support the encoding of odor identity in PCx. PAC occurred not only at a variety of theta phases but also at a variety of modulating/modulated frequency combinations (within the theta and gamma bands, respectively), providing a multi-dimensional physiologic substrate for neural coding[9,12]. We hypothesized that both the frequency and phase specificity of odor-induced nested oscillations would be important for odor coding in PCx (i.e., a frequency and phase code). To test this, we used a machine learning approach to decode odor identity from each single-trial oscillatory response to cue odors.

To do this, each trial was represented by the overall pattern of theta-coupled gamma, in which the distribution of gamma power was computed across three axes (see single-trial e.g. in Figure S4A): (i) 20 sub-bands of the modulated gamma oscillation; (ii) 11 sub-bands of the modulating theta oscillation; and (iii) 60 phase bins of the modulating theta oscillation. We implemented a non-linear support vector machine[48] (SVM) classifier (ten odor types, resulting in chance-level accuracy of 10%), using a leave-one-out cross-validation technique on the set of all cue odor trials. In this way, we found that odor-induced patterns of theta-coupled gamma in PCx were stimulus specific, with significant decoding achieved ($p < 0.05$ relative to surrogate distribution constructed by shuffling odor labels) in five of the seven subjects (dashed bars in Figure 4). We emphasize that odor identity could be decoded from PCx irrespective of specific sequence positions in which the cue odors were presented. In contrast, in parallel analyses, odor identity could not be reliably decoded from AH, with significant decoding limited to one out of six subjects.

To further corroborate that odor identity was represented in PCx with a frequency and phase code, we performed two control analyses. First, we systematically reduced the dimensionality of the original feature space (see Methods) to construct five alternative feature spaces depicting the pattern of theta-coupled gamma (see summary table in Figure 4): for example, information on theta phase specificity (axis iii) was removed, leaving a feature space describing only the frequency specificity of theta-gamma PAC (Figure S4B); as another example, information on both gamma and theta frequency specificity (i and ii) were removed, resulting in a single theta phase distribution of gamma power (Figure S4E). To control for differences between feature spaces, surrogate distributions were built independently for each format, which were used to *z*-score normalize the observed raw decoding accuracies. At the group level, the normalized decoding accuracies with the full three-dimensional feature space were greater than for each of the reduced-dimension feature spaces (paired-sample *t*-test, $p < 0.02$; Figure 4), suggesting that both the frequency and phase specificity of theta-gamma PAC contribute to PCx odor coding.

Second, to demonstrate that the pattern of gamma with respect to theta carried the most relevant information for PCx odor coding, classification was attempted using the temporal pattern (relative to stimulus onset) of odor-induced gamma activity (see Methods). We also performed classification with the temporal pattern of theta, as well as of both theta and gamma (but without any explicit reference to cross-frequency relations). Model performance was likewise worse than with the three-dimensional feature space depicting theta-coupled gamma (paired-sample *t*-test, $p < 0.05$; Figure S4F).

Finally, note that odor identity could not be decoded in any subject using a one-dimensional distribution of gamma power across theta phase, devoid of information on the specific sub-bands within theta and gamma that are coupled. In contrast, the demonstration of a consistent and separable theta phase preference depending on sequence position suggested a theta phase code of temporal order. In parallel decoding analysis, we found congruent evidence that, in both PCx and AH, sequence position could be decoded with the feature space depicting only the theta phase specificity of theta-gamma coupling (Figure S4G). Moreover, the addition of information on theta frequency and gamma frequency specificity (i.e, the three-dimensional feature space of theta-coupled gamma) did not lead to a significant difference in model performance (two-tailed paired-sample *t*-test; in PCx, $t_6 = 1.33$, $p = 0.2$; AH, $t_5 = 1.30$, $p = 0.3$), suggesting that the pertinent features driving classification of sequence position was the theta phase specificity of theta-coupled gamma.

Reactivation of experienced odors during maintenance

Insofar as the identity of cue odors could be distinguished based on stimulus-driven patterns of theta-coupled gamma in PCx, we next asked whether these odor-specific patterns would be spontaneously reinstated during the delay period. Hence, in the following classification analyses, odor-induced spectral patterns from the encoding period continued to serve as the training set (using all cue odor trials irrespective of behavior), whereas theta-coupled gamma patterns extracted from the delay period served as the test set.

In an initial analysis, we computed the pattern of theta-coupled gamma for each maintenance trial using data from the entire epoch. Given that each sequence comprised three odors, model performance was compared for the three *in-trial* odors retained during the delay period vs. the remaining seven *out-of-trial* odors. Across all maintenance trials, we observed higher decoding accuracy for in-trial vs. out-of-trial odors (raw accuracy 12.5 ± 0.8% vs. 9.9 ± 0.4%; paired-sample *t*-test, $t_6 = 3.37$, $p = 0.01$; Figure 5). Note that decoding of the out-of-trial odors was at chance level of 10%. Furthermore, if odor-specific delay activity is important for behavior, then on a subject-by-subject basis, a higher level of representational precision (as indexed by decoding accuracy) should be associated with enhanced performance on the odor identity match judgment. Indeed, decoding accuracy during successful odor identity maintenance (15.0 ± 0.7%) was greater than during all maintenance trials ($t_6 = 3.79$, $p = 0.009$).

To ensure that these results were not driven solely by reverberations of the oscillatory response to the third cue odor (see legend of Figure 1A), decoding was performed for odors in each of the three positions separately (using the set of identity match correct trials), all of which resulted in higher accuracy compared to the out-of-trial odors (paired-sample *t*-test; first sequence position, $t_6 = 2.56$, $p = 0.04$; second, $t_6 = 3.53$, $p = 0.01$; third, $t_6 = 3.55$, $p = 0.01$). Decoding accuracies across the three positions were also no different from each other ($p > 0.2$). Together, these data suggest that experienced cue odors are reactivated in PCx during memory maintenance, with direct relevance for subsequent memory-guided judgments.

Replay of experienced odor sequences during maintenance

Next, we tested whether the convergence of odor coding and temporal order coding would give rise to mnemonic representations that preserve both the "what" and "when" of odor sequences. In formulating this hypothesis, we drew from the rodent literature[26–29], and from recent findings in humans[49–52], showing endogenous reactivations of past sequential experiences in a temporallycompressed format, i.e., memory replay. We assessed for replay in PCx via time-resolved decoding of delay activity, whereby the classifier was again trained on cue odor-induced patterns of theta-coupled gamma, but now applied to each test instance (200-ms sliding windows with 90% overlap) spanning the maintenance period to depict the time course of reactivations for each of the three experienced cue odors. Visual inspection of these reactivation time series in individual trials revealed discrete neural events, temporally compressed across multiple successive theta cycles, in which spectral patterns specific to each of the recently encoded sequence odors were replayed in the same order as in the original experience (Figure 6A).

To provide statistical evidence for the presence of replay, we used the "sequenceness" metric[49,53] to quantify the degree to which reactivations of each memory item reiterated the original 3-item sequence, in either the forward or reverse direction. Sequenceness was quantified across a range of potential time lags between successive cue odor reactivations ([20, 600] ms), and significance was assessed relative to surrogate data generated from the four permuted 3-item (non-sequential) sequences (see Methods). At the group level, we found evidence for forward sequenceness with an inter-reactivation time lag of 160–260 ms (Bonferroni-corrected across time lags, $p < 0.05$; Figure 6B). Insofar as cue odors were presented at 4–5 s intervals during encoding, replay demonstrated a 15–30 fold temporal compression. To validate that these effects were task-related, we repeated this analysis on data from the pre-encoding baseline period, immediately prior to experiencing odor sequences, and found no evidence for sequenceness (Figure 6C).

Although replay events could be identified in maintenance trials across all behavioral conditions, we asked whether the prevalence of replay events would be predictive of subsequent memory. Pooling trials across subjects, we found that replay events were more common prior to a correct performance on both the identity match and sequence position judgments (75% vs. 53%, Fisher's exact test, $p < 10^{-4}$). We assessed the robustness of this finding using a bootstrapping approach. Across 10,000 bootstrapped subsets of trials, we correlated the number of replay events with the percentage of correct trials. This procedure was repeated 1,000 times, generating a distribution of Pearson's r (across repetitions, $p < 10^{-26}$; Figure 6D). We found that there was a positive correlation between the two variables, which was stable across repetitions (95% CI of r [0.12, 0.15]), confirming the statistical significance of the behavioral correlation.

Odor sequence replay is coordinated by the theta rhythm

During replay, the time lag between individual cue odor reactivations was concordant with the duration of a single theta cycle, indicating *cycle-specific packaging* of the "what" of odor sequences (as illustrated in Figure 6A). To address prior work showing that stimulus-specific neural activity during the delay period is also locked to *distinct phases of theta*[19,21,54,55],

we asked whether the theta phase preference of cue odor-induced gamma during their encoding would be preserved during their cycle-specific replay. Note that these two effects can co-exist, as evidenced by organization of spatial memories in rodents across both phase and cycles[26,28,29].

In order to determine the preferred theta phase of each cue odor reactivation, we first identified individual replay events for an inter-reactivation time lag of 200 ms (see Methods; Figure S5A). Each 600-ms replay event ([−100, 500] ms with respect to replay onset) was then partitioned into three 200-ms epochs, from which we derived the overall phase preference of each cue odor reactivation, closely mirroring the phase separability analysis during encoding (see illustration in Figure S5B-D). We found that the preferred theta phases of reactivations were separable for all three pairwise tests (position 1 vs. 2, 2 vs. 3, 1 vs. 3) in six out of seven subjects (Watson-William test, $p < 0.05$). To confirm that this was not a trivial result of sampling theta phase values across the three contiguous epochs, we confirmed significance relative to a surrogate distribution of test statistics constructed from randomly sampled time windows throughout the included maintenance trials, which gave qualitatively identical results ($p < 0.05$; Figure S5E). These data suggest that during replay, memory items were separated across multiple theta timescales, i.e., across both phase and cycles.

On the other hand, information on the “when” of odor sequences was preserved by linking the three cycle-specific constituents across consecutive theta cycles, while recapitulating the original sequence order. The presence of replay, therefore, implies a degree of control over neural processing spanning multiple oscillatory cycles. Given the essential role of the hippocampus in temporal order memory[1,2], we examined whether replay identified in the PCx would be associated with enhanced cross-structural theta-band synchrony with the AH, as a potential mode of inter-regional communication[35].

We quantified theta synchrony during individual replay events with the phase-locking value[56] (PLV). We generated a baseline distribution for each maintenance trial by computing PLV for randomly sampled time windows of the same 600-ms duration, which was then used to *z*-score normalize the observed PLV during replay events. The normalized PLV was greater than zero in all five subjects (one-sample *t*-test; PLV, $t_4 = 8.68$, $p < 0.001$). These temporally specific increases in theta synchrony were independent of changes in theta power in either region: within-subject, cross-trial Pearson’s r of PLV vs. PCx theta power was not significant (r [−0.21, 0.12], $p > 0.1$), and likewise for AH theta power ([−0.12, 0.08], $p > 0.3$). Furthermore, to confirm that PCx-AH synchrony was not a general effect, we quantified theta phase synchrony between PCx and an anatomic control region, for which we used the lateral temporal cortex (LTC; Figure S1). At the group level, PCx-LTC synchrony was no different from zero (PLV, $t_6 = 0.45$, $p = 0.6$). Finally, we confirmed the robustness of these results with an alternative measure of phase synchrony that is thought to be less sensitive to spurious increases from volume conduction, phase lag index[57], which gave qualitatively identical results.

DISCUSSION

The encoding and maintenance of a newly encountered temporal sequence of stimuli in working memory (say, the aroma of honeysuckle, followed by pine, followed by mint) poses unique challenges for the brain. Both the individual stimuli and their relative timings within the sequence need to be represented, while mitigating interference between memory items. Here we show that nested theta and gamma oscillations within and between PCx and AH independently code for both the content ("what") and temporal context ("when") of odor sequences. Moreover, we found that theta oscillations, widely implicated in both olfactory[32,33,58] and mnemonic processing[10,11,35,59], separate odor information across theta phase, as well as across consecutive cycles during their short-term retention. Critically, the robustness of this segregation across multiple theta timescales was predictive of subsequent recall performance.

Theta-gamma PAC as a multiplexed coding scheme for sequence representations

Theta-gamma PAC has been well documented in human intracranial studies of memory, both for individual items[55,60–62] as well as for sequences[18–20,63–65]. Alongside these studies using visual stimuli, our data demonstrate that the functional significance of theta-gamma PAC generalizes across sensory modalities. During encoding of individual items, the pattern of stimulus-induced spectral power (across one dimension, namely frequency) has been shown to convey information on the category, and even the identity of memory items[24,25,42]. Although substantial experimental and theoretical work has focused on nested oscillations as a basis of multi-item sequence memory, how they contribute to sequence coding *per se* remains unclear. From a computational perspective, cross-frequency PAC allows for a dramatic increase in neural coding space across multiple dimensions (e.g., modulating phase, modulating frequency, and modulated frequency), which may be critical for representations of more complex memories[9,12]. Indeed, we found that coupled theta and gamma oscillations serve as a physiologic substrate for multiplexed representations of odor sequences: sequence position was represented with a theta phase-based code, independent of odor type, whereas odor identity information was conveyed by both the frequency and phase-specific patterns of theta-coupled gamma, independent of sequence position.

Moreover, in PCx, odor-specific oscillatory patterns from the encoding period (used to train our classifier) generalized to delay period data, implying that mnemonic information can be represented in limbic-based cortical areas in a sensory-like format. Our data accord well with the broader human neuroimaging literature demonstrating that neural regions and representations engaged during online processing of visual and auditory streams also contribute to their working memory maintenance[66–68]. Furthermore, the precision (i.e., discriminability) of odor-specific delay activity in PCx had direct relevance for subsequent identity recall, which aligns well with recent work in rodents showing that piriform delay activity is causally important in short-term retention of olfactory content[30].

Organization of odor information across theta phase and cycles

Our results build on accumulating evidence that theta oscillations have a central role in the coordination of neural activity such that multiple memory items sharing a common

neural substrate can be maintained in an active and discriminable state[10,11]. The underlying theoretical framework is that items are disambiguated by temporally separating the corresponding neuronal groups in theta phase space as well as across cycles[13–17]. Empiric support comes from rodent single-unit studies of spatial navigation, in which phase-specific spatial memory representations are concatenated across different phases within an individual theta cycle, giving rise to "theta sequences" that represent segments of the environment[27]. In turn, distinct cycle-specific representations are further organized across successive theta cycles[26,28,29], which has been proposed to underlie memory maintenance of an extended experience by linking its constituent segments together in time[10,11].

In humans, while segregation of memory items in theta phase space has been demonstrated[19,20,54,55], there has been limited evidence for organization across multiple theta timescales. In our study, individual odor representations during replay were compressed into timescales concordant with a single theta cycle, which were in turn concatenated across consecutive theta cycles while preserving the temporal structure of the original perceptual experience. In this way, our data provide unique human evidence for segmentation of mnemonic information across theta cycles, suggesting that individual theta cycles may be a functional unit in organizing neural representations, conserved across species and across information domains[11,69]. It remains unclear what advantages this theta timescale organization confers on brain function and, ultimately, behavior. Answering such questions will require experiments probing their downstream implications. For example, in rodents, disruption of theta-timescale dynamics of head direction cells (without changing their tuning) is associated with loss of spatial periodicity in downstream grid cells[26].

Our data are consistent with computational models in which sequential reactivation of memory items occurs at the timescale of theta cycles[13–15]. However, we note that our findings do not preclude the possibility that aspects of the encoded odor sequences are also being replayed within each theta cycle. As the feature space for odor identity was derived, in part, from the distribution of gamma with respect to theta phase, we identified replay using decoding time bins of 200 ms; hence, our methods were likely not optimal to resolve intra-cycle dynamics. Indeed, other models[16,17] have proposed that individual mnemonic items are reactivated during single gamma cycles, with the entire sequence being replayed across multiple gamma cycles nested within a single theta cycle. These models predict that the ratio between the frequency of the modulated gamma oscillation and the frequency of the modulating theta oscillation would increase with memory load, ostensibly to accommodate more memory items. However, empiric studies have not consistently established this effect[18,64,65]. Additionally, it is important to note that the demonstration of memory item-specific neural activity occurring at distinct theta phase ranges[19,21,54] does not necessarily imply replay of the entire sequence of items within individual theta cycles, as the phase preference can be expressed by neural activity within a single cycle or distributed across multiple cycles.

Replay in piriform coincides with cross-structural theta synchrony with hippocampus

A key question centers on how the brain is able to preserve the temporal context of sequentially-encoded odors during their replay. The hippocampus has long been implicated

as a major source of top-down signals that contribute to sequential reactivation of cortical representations[46,47,70]. In fact, coordinated sequential activity between the hippocampus and various cortical regions (entorhinal, visual, auditory)[71–73] has been observed in rodents, whereby neural activity in each structure reflects the same awake experience, preserving the original spatio-temporal sequence of events. Critically, hippocampal activity has been shown to be predictive of subsequent cortical activity during coordinated replay, suggesting a direction of information flow from hippocampus to cortex[72].

Phase synchrony constitutes a plausible physiologic mechanism supporting such long-range neural communication[35]. In particular, cross-structural synchrony in the theta band has been widely implicated during tasks in which information about objects/events must be integrated with information about their temporal or spatial contexts. For example, hippocampal-PCx theta synchrony correlated positively with performance on an odor identification task requiring rodents to keep track of inter-stimulus time intervals[32]. Similarly, during spatial-memory guided tasks, hippocampal-prefrontal cortex (PFC) theta synchrony peaks as rodents approach choice points, and was predictive of subsequent performance[74,75] (see also, ref[59]). Taken together, our data highlight the important binding role of phase synchronization, whereby representations stored in specialized cortical regions (e.g., PCx for sensory objects, PFC for abstract task-related variables) are embedded in a task-dependent contextual map, allowing for flexible memory-guided behavior.

Online replay supports working memory maintenance

During spatial navigation, two types of sequential activity are generated in the rodent hippocampus, either during periods of pronounced theta oscillations[26–29] or sharp-wave ripples (SWR)[71,72,76]. Theta sequences are observed while the animal is actively engaged in spatial navigation, i.e., in the online state. In contrast, SWR-related sequences, which are generated over even more compressed timescales (50–120 ms), have been observed in both online and offline states (i.e., during sleep or quiet rest). Furthermore, whereas the former has been mainly described as forward oriented, the latter exhibits both forward and reverse directionalities. While further research is needed to confirm any potential cross-species homologies, three features of the online replay identified in our study provide strong parallels and convergence with rodent theta sequences: first, replay emerges at the timescale of theta; second, replay exhibits forward directionality; and third, replay coincides with periods of enhanced synchrony with the hippocampal theta rhythm.

Although theta sequences in rodents have classically been proposed to support sequential memory encoding[10,17], they can also reflect future goal trajectories[28,77], suggesting a role in planning and prediction. Hence, it remains unclear whether the behavioral impairment observed in rodents during spatial navigation tasks with disruption of theta sequences is primarily related to a deterioration in memory processes, in decision making, or both[78]. Human research represents an opportunity to generate complementary data as subjects are able to verbally report their perceptions and experiences. Notably, the emerging human replay literature has demonstrated sequential reactivations of past experiences primarily in the offline state, following complex planning tasks[49–52]. In our study, online replay identified during working memory maintenance was predictive of subsequent recall

performance on a trial-by-trial basis, providing a novel link between endogenous replay and short-term memory retention in the human brain.

STAR METHODS

RESOURCE AVAILABILITY

Lead contact—Andrew I. Yang (iyang.and@gmail.com).

Materials availability—This study did not generate unique materials.

Data and code availability—Data are uploaded to a public repository (see Key Resources Table). Algorithms and codes used in analysis are available as open source as indicated in the STAR Methods (see Key Resources Table). Additional information is available upon reasonable request from the lead contact.

EXPERIMENTAL MODEL AND SUBJECT DETAILS

We recorded electrophysiological data from eight subjects (three males, five females; age 35, 34, 35, 27, 28, 40, 57, 39 yo) with intractable epilepsy who were implanted with intracranial depth electrodes for pre-surgical localization of seizure foci. Data were recorded from Northwestern Memorial Hospital (NMH) and Hospital of the University of Pennsylvania (HUP). Informed consent was obtained from all subjects in accordance with the local Institutional Review Boards.

METHOD DETAILS

Data acquisition—Electrode placement decisions were made exclusively on clinical grounds, and typically focused on areas in the medial temporal lobe. Overall, three subjects had bilateral medial temporal lobe electrodes, four subjects had right-sided electrodes only, and one had left-sided electrodes only. Depth macro-electrodes implanted at NMH (Integra LifeSciences, Plainsboro, NJ; Model 15819D508) and HUP (Adtech AG, Frankfurt, Germany; Model SD10R-SP05X-000) had similar dimensions. Each lead had 8–12 cylindrical platinum electrode contacts, with 2.4–2.5 mm of exposed surface, and a 2.5–2.6 mm gap between contacts. Data were acquired using a 128-channel Nihon Kohden recording system (Tokyo, Japan) at NMH and a 256-channel Natus recording system (Natus Medical Incorporated, Pleasanton, CA) at HUP. Signals were sampled between 500–2000 Hz at the physician's discretion for each subject across sites. Respiratory airflow data were simultaneously collected using a piezoelectric pressure sensor attached to a nasal cannula (Salter Labs, Vista, CA).

Recording locations—In addition to the human olfactory cortex (i.e., piriform cortex [PCx]), we recorded from the anterior hippocampus (AH). Overall, seven subjects had PCx electrode coverage, six had AH coverage, and five had coverage in both regions. Our choice to focus on the anterior, as opposed to posterior, hippocampus was based on the following considerations: 1) converging evidence suggests that the anterior/ventral hippocampus in primates/rodents are selectively involved in non-spatial cognitive processes, including higher-order relational memory[79,80]; 2) this sub-region is also selectively involved

in processing odor information[33,34,81,82]; 3) previous empiric support for oscillations underlying human sequence memory were based on recordings primarily from the AH[18].

Electrode selection—After co-registering the pre-operative high-resolution MRI with the post-operative CT using a linear affine registration[83], electrodes were localized in native space, and then transformed to Montreal Neurological Institute (MNI) space for across-subject visualization on an average MNI-152 brain. Electrodes in PCx or AH were first determined based on visual comparison with manually-drawn regions of interest in MNI space. Subsequently, to control for variability in electrode coverage, for each subject we chose two PCx electrodes closest to the sub-region of greatest activation during odor processing, as identified in a meta-analysis of human neuroimaging studies[81]. We likewise chose, in each subject, two AH electrodes with the largest theta-gamma PAC strength during task periods (see Phase-amplitude coupling). Previous recordings in the human hippocampus have shown theta-gamma PAC during working memory processes[18,20,62,64]. Although primarily observed in the anterior aspect of the hippocampus, this measure has not been further localized to any specific anatomic sub-region. Finally, we chose the lateral temporal cortex as an anatomic control region, for which we selected, in each subject, the most superficial electrode on the same lead as for the PCx/AH electrodes (Table S1).

Behavioral paradigm—We devised an olfactory version of the three-item Sternberg working memory task[36], in which three odor items (cues) were presented serially, followed by a brief delay, and concluded with a test odor (probe). Odors were selected pseudo-randomly from a set of ten unique and discriminable odor stimuli (anise oil, cinnamon, coffee, honeysuckle, mint, orange, peanut butter, pine, strawberry, vanilla) and were administered via a custom-built, twelve-channel olfactometer, with two additional channels delivering clean air. The olfactometer was controlled using a computer equipped with MATLAB (MathWorks, Natick, MA), and the experiment was designed and administered using the MATLAB package PsychToolbox[84].

Each trial began with a fixation cross lasting 4–5 seconds (pre-encoding baseline). Subsequently, three different odor cues were presented sequentially (encoding). For each odor, subjects were cued to sniff, sampling each odor for one second, with 3–4 seconds between odor deliveries to allow enough time for natural expiration. After presentation of the third cue odor, a retention period lasting 7–10 seconds was observed (maintenance), after which subjects received the probe odor (retrieval). In 50% of trials, the probe matched one of the three cues, for which the probe matched the cue odors in each of the three sequence positions in roughly equal proportions. In the remaining 50% of trials, the probe was a novel odor not matching any of the in-trial cues. Moreover, across the experiment, each unique odor type was presented in roughly equal numbers in each of the three cue positions, as well as across probes.

Subjects performed up to two judgments on the probe odor. First, subjects selected whether the probe odor was novel or previously encountered (identity match judgment), where an accuracy of 50% would suggest no recollection/random guessing. The behavioral outcomes for the first probe judgment were: 1) hit (stating “yes” when the probe was in the sequence); 2) false alarm (FA; “yes” when the probe was *not* in the sequence); 3) correct rejection (CR;

"no" when the probe was *not* in the sequence); or 4) miss ("no" when the probe was in the sequence). Second, if subjects responded that the probe matched one of the cues (hit or FA), they then reported whether the first, second, or third cue odor in the sequence matched the probe (sequence position judgment; chance level accuracy 33%). As there was no ground truth for the sequence judgment after a FA response, there were two behavioral outcomes after the second probe judgment: 1) hit trials with correct sequence position judgment; or 2) hit trials with incorrect position judgment. If the subject reported that the probe was novel (CR or miss) the experiment moved to the next trial. Each subject performed a total of 50–60 trials.

Identity match accuracy was defined as the percentage of hit or CR responses across all trials, and sequence judgment accuracy as the proportion of hit + sequence correct responses among all hit trials. To determine identity match accuracy across subsets of trials in which the probe odor matched the cue odor presented in the first, second, or third sequence positions, we calculated, within each subset of trials, the percentage of hit responses among all hit or miss trials. Consistent with prior human behavioral data[5], two subjects demonstrated a recency effect on the odor identity match judgment (accuracy for trials in which the probe matched the first or second cue odors vs. the third; S7, 31% vs 78%, Fisher's exact test, $p = 0.04$; S8, 44% vs 100%, $p = 0.008$), whereas no subject demonstrated recency on the sequence position judgment. Notably, the one (and only) subject who performed near chance level in the odor identity match judgment (S7) demonstrated recency, suggesting that this subject was not merely guessing. Moreover, electrophysiologic data from S7was limited to AH, i.e., this subject had no electrode coverage of PCx.

Data pre-processing—All data were analyzed offline in MATLAB using custom scripts in conjunction with functions from the EEGLAB toolbox[85]. Data were down-sampled to 500 Hz (after an anti-alias filter), and then high-pass filtered at 0.1 Hz using a two-way least-squares zero phase-lag finite impulse response (FIR) filter (eegfilt.m from EEGLAB). Data were then notch-filtered at 60 Hz and its harmonics to remove line noise using a second-order infinite-impulse response (IIR) filter. All channels were visually inspected. Noisy and flat channels in which the mean magnitude of the signal (mean of the absolute value of raw amplitudes) was 3 s.d. above or below the mean across channels were rejected, as well as channels with abnormal or interictal spikes. We also eliminated all extra-parenchymal electrodes based on visual inspection in native space. After electrodes rejection, each remaining electrode's LFP signal was then referenced to the common average (i.e., average signal across all electrodes) to reduce common noise (e.g., from volume conduction and remote field effects). While bipolar referencing is superior to common average referencing in reducing inter-electrode signal correlation from common noise, our choice of common referencing was motivated by the fact that bipolar referencing can lead to phase distortion, signal mixing, and signal cancellation[86,87].

Data during the encoding and retrieval periods were aligned to the onset of sniff in the presence of odor stimuli to three seconds after. Data from the maintenance period were aligned from one second after the end of the inhalation phase in response to the third cue odor to four seconds after. An equivalent-length baseline period was defined for each trial, from the time period prior to presentation of the first cue ([−3.5, −0.5] s relative to

onset of first cue odor). All analyses were conducted with the 3-s epochs defined above, unless otherwise noted. We then performed artifact rejection at the trial level, using 100-ms sliding windows (with 50% overlap). Any trials containing a bin in which the mean signal magnitude exceeded 5 s.d. above or below the mean across bins and trials (within electrodes) were rejected. Across subjects, 86.7% ± 2.7% [77, 95.5] % (mean ± s.e.m. [range]) of trials were retained after trial rejection from PCx electrodes, and 92.2% ± 1.9% [85, 97.3] % of trials were retained from AH electrodes.

Respiratory data were low-pass filtered at 10 Hz and manually inspected. Odor stimulus trials (cue and probe odors) in which inspiration was sub-optimal were rejected if any of the following conditions were met: 1) overlap between odor and inhalation < 100 ms; 2) peak velocity of inspiration < 5^{th} percentile of the distribution of peak velocities across all odor trials (within subjects); 3) two successive rapid sniffs taken during the 1-s odor delivery period.

QUANTIFICATION AND STATISTICAL ANALYSIS

As noted above in **Recording locations**, data were acquired from a relatively small number of subjects. Therefore, we focused our analyses on demonstrating the consistency of our findings across subjects, with the use of within-subject statistical tests. Furthermore, all group-level results were based on one data point from each subject. Trials were combined across the pair of electrodes in each region of interest for within-subject analyses, unless otherwise noted. Finally, all statistical tests were two-tailed with $\alpha = 0.05$ or one-tailed with a corrected α.

Oscillatory power—Theta-band power was computed from the spectrograms (pwelch.m) of each task period (cue odors 1, 2, 3, maintenance, probe odor), using a published method "fitting oscillations & one over f", which iteratively identifies oscillatory peaks and extracts their height with respect to the aperiodic $1/f$ component[44] (see Figure S2A-B). This data-driven method does not require any *a priori* assumptions regarding the frequency bands of interest. First, the aperiodic portion was approximated with a least-squares linear fit in log-log space, with a fitting range of 0.1 to 40 Hz to exclude 60 Hz line noise, as well as to stay below the bend in the aperiodic signal at 70 Hz identified in human intracranial data[88]. The aperiodic portion was then removed, and the residual signal (assumed to be mix of oscillatory peaks and noise) was z-score normalized with respect to itself. From the residual signal, an oscillatory peak was identified at the local maximum only if it met a threshold criterion of 2 s.d. greater than the mean. The oscillatory peak, if any, was then fitted with a Gaussian, which was removed from the residual signal. This process is repeated until all supra-threshold oscillatory peaks were identified and removed. We then returned to the raw spectrogram, from which all Gaussian fits of oscillatory peaks were removed, and the final fit of the aperiodic component was repeated in log-log space. Finally, we repeated the procedure to identify oscillatory peaks with the final fit of the aperiodic component. The overall fit of the spectrogram (both the aperiodic portion and any oscillatory peaks) was statistically assessed with the F-test, which were highly significant for all task periods in all subjects (PCx, $p < 10^{-16}$; AH, $p < 10^{-11}$). From the spectrograms of each task period, we reported the power (local maximum of residual signal) and center frequency of the largest

oscillatory peak, if any. Three subjects had secondary peaks: in PCx, S3 had a 12 Hz peak during cue 2, and S4 had 8–9 Hz peaks during cue 2/3/probe; in AH, S6 had 6–7 Hz peaks during all task periods. Importantly, in each of these instances, there was a primary peak in the theta frequency range.

For single-trial depictions of spectral power across time and frequency, raw traces were filtered between 1 and 200 Hz at 60 center frequencies increasing logarithmically (50% overlapping bandwidths), again using a zero phase-lag FIR filter. Subsequently, the Hilbert transform was applied to extract the instantaneous amplitude at each time point and frequency bin. We then *z*-score normalized power in each frequency with respect to the pre-encoding baseline.

Phase-amplitude coupling—Phase-amplitude coupling (PAC) was quantified with a published "oscillation-triggered coupling" method[40,42] (see Figure S2), which offers the unique advantage of accounting for amplitudemodulated high-frequency oscillations occurring in the form of discrete neural events (as in our data; see Figure 2A). Specifically, the statistical relationship between the timing of such events to the phase of concurrent modulating low-frequency oscillations was quantified with the *modulation strength* metric. Additionally, this method allows identification of the predominant modulating and modulated frequencies across a broad range of candidate frequencies (1–10 Hz and 20–200 Hz for modulating and modulated oscillations, respectively).

For each subject × region of interest, PAC was evaluated independently for each narrow-band oscillation whose center frequencies spanned the modulated frequency range of interest (42 sub-bands from 22 to 186 Hz with 4 Hz steps; bandwidths linearly increased from 6 to 50 Hz). Power was extracted from the bandpass-filtered signals of each trial, which were then *z*-score normalized with respect to the pre-encoding baseline. We then performed the following steps (for each evaluated modulated sub-band) to quantify the modulation strength and determine the frequency of the associated modulating oscillation. First, we identified periods of enhanced activity (max normalized power > 2 s.d. from mean power during pre-encoding baseline) that was sustained for more than three oscillatory cycles (onset/offset defined as 10% of max power). Second, the center times of all identified oscillatory events were used as trigger time points to extract the peri-event raw LFP signals ([−1, 1] s), which were averaged across events to compute the *modulatory signal*. The max peak-to-trough distance of the modulatory signal was treated as the raw modulation strength. Third, surrogate data was generated by repeating the above procedure at trigger time points randomly selected throughout the experimental trace (N = 1,000), with statistical significance achieved if the observed raw modulation strength was > 99.94th percentile of the surrogate distribution (corresponding to a one-tailed threshold of $p < 0.025$ after Bonferroni correction across the 42 modulated sub-bands). PAC strength was reported after *z*-score normalizing the observed raw modulation strength with respect to the surrogate distribution. Forth, the spectrogram of the modulatory signal was inspected to identify the predominant modulating frequency, if present. To do this, we followed the same procedure used to identify oscillatory peaks in the power spectra of each task period (see Oscillatory power). After removal of the aperiodic portion across the fitting range of 0.1 to 40 Hz, a modulating frequency was determined if 1) the largest peak was within the modulating

frequency range of interest (1–10 Hz), and 2) if the maximum met the same threshold criterion (i.e., 2 s.d. greater than the mean of the normalized residual signal).

We performed the following comparisons of theta-gamma PAC strength: 1) encoding (cue 1/2/3) and maintenance vs. pre-encoding baseline; 2) during encoding and maintenance, identity match-correct (hit + CR) vs. incorrect (FA + miss) trials. We combined trials across encoding and maintenance to ensure a sufficient number of events for non-parametric statistics using surrogate data, which for LFP data is ≈ 70 events per condition[40]. Moreover, as there were more than one significant theta phase-modulated sub-band within the gamma frequency range (for each subject × region of interest), we performed the above two comparisons for the modulated sub-band associated with the strongest modulation by theta phase (determined independently for each subject × region of interest). Importantly, selection of the modulated sub-band was conducted on the combined set of oscillatory bursts identified (with the power and duration criteria) across the two conditions being compared (i.e., baseline + task periods for the first comparison, or identity-correct + incorrect task periods for the second). The specific modulated sub-bands selected in this way were all within the gamma frequency range: in PCx, there were 115 ± 11, 293 ± 51, and 95 ± 15 gamma bursts identified during baseline, identity-correct task periods, and identity-incorrect task periods, respectively; In AH, there were 138 ± 26, 377 ± 67, and 128 ± 25 gamma bursts. To compare modulation strengths of gamma bursts between the two conditions, we then re-computed modulation strengths (for the selected modulated sub-bands) separately for gamma bursts detected during each condition. For example, for the first comparison, modulation strength was computed separately for gamma bursts during task periods vs. during baseline. To control for differences in the number of gamma bursts across the two conditions, we used a resampling procedure (N = 1,000), whereby at each iteration we randomly sampled the minimum number of gamma bursts. Likewise, in generating surrogate data, we randomly sampled the same number of trigger time points at each iteration. Burst duration was reported based on the same set of modulated sub-bands, selected for each subject × region of interest as described above. Of note, the average prevalence of gamma bursts, quantified with the temporal rate of occurrence, was as follows: in PCx, 0.61 ± 0.04 s^{-1}, 0.59 ± 0.05 s^{-1}, 0.59 ± 0.05 s^{-1}, and 0.61 ± 0.05 s^{-1} during baseline, task periods, identity-correct task periods, and identity-incorrect task periods, respectively; in AH, 0.59 ± 0.04 s^{-1}, 0.58 ± 0.04 s^{-1}, 0.58 ± 0.04 s^{-1}, and 0.55 ± 0.04 s^{-1}.

Theta phase coding of sequence position during encoding—We evaluated whether gamma activity induced by cue odors occurred at distinct phases of the underlying theta oscillations depending on its position within the 3-item sequence. For each cue odor trial, we computed the distribution of gamma power across theta phase (60 non-overlapping phase bins spanning $[-\pi, \pi]$). To focus on stimulus-driven dynamics, we *z*-score normalized odor-induced gamma with respect to the pre-stimulus baseline ([−1, 0] s), and used data from the first 1.5 seconds after stimulus onset. We then assessed both the cross-trial *consistency* of preferred theta phases within each sequence position, as well as the *separability* of preferred theta phases between each unique pair of sequence positions (i.e., position 1 vs. 2, 2 vs. 3, 1 vs. 3). We note that PCx data from one subject (S4) was excluded

for these analyses due to an insufficient number of trials (< 5 trials across sequence position × behavioral condition).

To assess cross-trial phase *consistency*, we averaged the theta phase distributions across cue odor trials within each of the three sequence positions. We then identified significant clusters of odor-induced gamma activity across contiguous theta phase bins, indicating a consistent theta phase preference across trials, using a surrogate data approach with cluster-level statistics[89]. Surrogate data was generated by shuffling the gamma power time series for each trial across time points while the theta phase time series was kept as is, allowing us to selectively alter the relation between gamma power and theta phase. This procedure was repeated 1,000 times, and the resulting surrogate distribution was used to *z*-score normalize the trial-averaged phase distribution of gamma power within each phase bin. Gamma power in each bin was then thresholded at 1 s.d., and positive cluster-level *z*-statistics were compared with respect to the surrogate distribution of maximum cluster-level *z*-statistics (one-tailed, $p < 0.025$). For behavioral correlations, we compared data for sequence correct (PCx, 18.14 ± 1.42 trials across all three sequence positions; AH, 19.06 ± 1.38) vs. incorrect trials (PCx, 12.81 ± 1.69; AH, 13.44 ± 1.79). To control for the different number of trials across behavioral conditions, we resampled the minimum number of trials 1,000 times to compute the trial-averaged phase distribution. We note that for each region of interest × behavioral condition, there was only up to one significant phase cluster for each subject × sequence position, with the exception of the following three instances: for sequence correct trials in AH, S2 had a secondary cluster for the second sequence position; for correct trials in PCx, S3 had a secondary cluster for the second position; for incorrect trials in PCx, S6 had a secondary cluster for the second position.

To assess the *separability* of preferred theta phases between sequence positions, i.e, how distinguishable the preferred phases were within theta phase space, the overall phase preference of odor-induced gamma was derived for each individual trial. To do this, we thresholded normalized gamma power in each single-trial theta phase distribution at 1 s.d., and then computed the weighted circular mean of the phase cluster with the largest cluster-level *z*-statistic, the angle of which was treated as the overall preferred phase. We applied the Watson-William test (a circular analogue of the two-sample *t*-test[90]) to compare the preferred theta phases between each unique pair of sequence positions. To control for different trial numbers across sequence position × behavioral condition, we used a resampling procedure (N = 1,000), and performed a parametric test on the mean *F*-statistic obtained across resampled sub-sets of trials. Importantly, at each resampling, the Watson-William test was only conducted if the mean resultant length of the phase values for each of the two sequence positions being compared was greater than a pre-specified threshold that was more stringent for smaller sample sizes (0.45 if ≥ 11 samples per sequence position, 0.5 if 7–10 samples, 0.55 if < 5 samples[90]). This was necessary to prevent spurious detection of phase differences between sequence positions occurring in the absence of a consistent phase preference (across trials) for each sequence position.

Decoding odor identity from cue odor-induced patterns of theta-coupled gamma—To investigate whether patterns of cue odor-induced theta-coupled gamma in PCx were stimulus-specific, we performed decoding of odor identity from individual cue

odor trials. Each cue odor trial was represented by the overall pattern of theta phase-coupled gamma power, by computing the distribution of modulated oscillation power across phases of the modulating oscillation for all pairs of modulating and modulated frequency sub-bands spanning the theta and gamma frequency ranges, respectively (see Figure S4A). In this way, each cue odor trial was represented with 13,200 features describing gamma power across three axes: i. 20 sub-bands of the modulated gamma oscillation (same center frequency/bandwidth as for the PAC analysis), ii. 11 sub-bands of the modulating theta oscillation (step 0.5 Hz, bandwidth 2 Hz), iii. 60 non-overlapping phase bins of the modulating theta oscillation. The resultant pattern was *z*-score normalized with respect to itself to control for absolute differences in gamma power across trials. Successful decoding of odor identity with this feature space would be consistent with a frequency and phase code for odor identity.

Decoding was performed using a multi-class (ten-way) non-linear support vector machine (SVM) with a radial basis function kernel[48]. As cue odors were randomly selected from a set of ten unique odor types, chance-level accuracy was 10%. Following our previous study[33], we accounted for the variable electrode sampling, across subjects, of each region of interest, by developing classifier models independently for each electrode. For each subject × region of interest, we reported data from the electrode with the higher decoding accuracy (of the pair of electrodes in each region of interest). Model accuracy was determined using a leave-one-out cross-validation technique to train on all but one random set of trials from each of the ten cue odor identity types, and tested on the left-out set of trials. We repeated this procedure 1,000 times, and reported the mean of the resulting distribution of decoding accuracies. At each iteration, the minimum number of trials across odor identities was sampled for the training set to ensure that the classifier would not be biased by sample size.

To justify the format of our feature space, we compared model performance with alternate feature spaces depicting the pattern of theta-coupled gamma, in which information along one or two of the three axes were systematically removed (see Figure 4, S4B-E). The resulting four feature spaces depicted the pattern of theta-coupled gamma across: 1) gamma frequency (axis i) and theta frequency (ii), which was therefore devoid of information on the theta phase specificity of theta-gamma coupling; 2) gamma frequency (i) and theta phase (iii), without information on the theta frequency specificity of coupling; 3) theta frequency (ii) and theta phase (iii), without information on the gamma frequency specificity of coupling; 4) theta phase (iii), without information on both the theta frequency and gamma frequency specificity of coupling. Note that the feature space #4 corresponds to the theta phase distribution of gamma power utilized in the previous analysis of sequence position (see Theta phase coding of sequence position during encoding), which was also used to perform a similar decoding analysis of sequence position (detailed in the next section). Dimensionality was reduced in one of two ways. First, gamma power was averaged across the axis/axes that were removed. For example, for feature space #3, we averaged gamma power across the 20 sub-bands of gamma for each of the 660 pairs of theta frequency sub-band × theta phase bin. Note that the total number of features would be reduced with this approach. Second, specifically for feature space #1, we also constructed the feature space by shuffling gamma power across theta phase bins within each of the 220 phase distributions (for each pair of theta sub-band × gamma sub-band). Note that this method preserves the overall size of the feature space. Finally, as an additional control feature space,

we shuffled gamma power across all three axes in two steps: phase distributions were first shuffled within itself, and then these phase distributions were further shuffled across the 220 pairs of theta sub-band × gamma sub-band.

Whereas each of the above feature spaces depicts the pattern of gamma power with respect to theta, we also performed classification with the temporal pattern of cue odor-induced oscillations. We extracted the pattern of spectral power across time and frequency in the theta band alone, in the gamma band alone, and in both the theta and gamma bands. We used the same frequency parameters as in the single-trial depictions of spectral power across time and frequency (see Oscillatory power), resulting in 12, 18, and 30 frequency sub-bands for theta, gamma, and theta + gamma, respectively. Note that in the third feature space, there was no explicit link made between the magnitude of gamma activity and theta phase. Following our previous study[33], time-frequency features corresponded to the mean power in each frequency sub-band spanning theta and/or gamma, calculated across non-overlapping 10-ms windows spanning the 3-s post-stimulus epoch.

For statistical testing, surrogate data was generated by shuffling odor identity labels across cue odor trials (N = 1000). Specifically, at each iteration, we built a classifier model with permuted labels, and then decoded for the permuted labels in the left-out set of trials. Importantly, in generating surrogate data, the feature space of each trial was not altered. Significance was assessed (within electrodes) by evaluating the proportion of accuracies from the surrogate distribution that exceeded the true model accuracy (one-tailed, i.e., significant if > 97.5^{th} percentile of surrogate distribution). To control for differences across features spaces (e.g., the number of features), we constructed surrogate distributions for each feature space separately, which were used to *z*-score normalize the observed raw decoding accuracies, allowing us to compare classification results across features spaces.

We tested whether cue odor identity decoding accuracy was different across behavioral conditions. To assure a sufficient number of trials (≥ 5) across odor identity × behavioral condition with electrode-level analysis, we compared decoding accuracy for identity-correct trials vs. all trials. Across subjects, there were a total of 12.69 ± 0.84 cue odor trials per odor type, of which 9.76 ± 0.69 were correctly encoded. We found no statistical difference across behavioral conditions (paired-sample *t*-test, $t_6 = 0.5$, $p = 0.6$), and therefore used the set of all cue odor trials for the current as well as subsequent odor decoding analyses.

Decoding sequence position from cue odor-induced patterns of theta-coupled gamma—We investigated whether sequence position could be decoded from single-trial oscillatory responses to cue odors in the PCx or AH (chance level = 33%), mirroring the previous odor identity classification analysis. For the set of sequence position correct cue odor trials, each trial was represented by the pattern of theta-coupled gamma across theta phase (axis iii) only (i.e., feature space #4 above). To provide further evidence for a theta phase code of temporal information, sequence position decoding was also performed using the full three-dimensional feature space depicting the pattern of theta-coupled gamma across gamma frequency (i), theta frequency (ii), and theta phase (iii)

Decoding odor identity from theta-coupled gamma patterns during maintenance—We used the model trained with cue odor-driven patterns of theta-coupled gamma to assess for reactivations of oscillatory patterns specific to the experienced in-trial cue odors during maintenance. Specifically, the classifier was trained with data from all cue odor trials (irrespective of behavior), and then tested on patterns of theta-coupled gamma extracted from individual maintenance trials. As in the previous classification analysis, at each iteration, we resampled the minimum number of cue odor trials across odor types to construct the training set. We then tested on a random subset of maintenance trials comprised of the same number of instances for each odor identity × behavioral condition (identity-correct trials vs. all trials). As there were three in-trial odors that are retained during each individual maintenance trial, at each iteration, decoding was performed for the identity of cue odors presented in each of the three sequence positions separately. Classification was also attempted for the identity of one of the remaining seven out-of-trial odors, in which the odor identity label for each trial was chosen randomly at each iteration while keeping the total number of instances per odor identity the same as for decoding of in-trial odors. This allowed comparison of model performance with respect to the cue odors presented in each of the three sequence positions or with respect to all in-trial odors (by taking the average of the decoding accuracies obtained across the three sequence positions).

Statistical test of replay—We implemented a time-resolved decoding analysis of PCx delay activity to determine if cue odor reactivations reiterated the temporal order of the originally-experienced sequence. In the above classification analysis of delay activity, theta-coupled gamma patterns for each maintenance trial were extracted from data across the entire 3-s epoch. In contrast, for the current analysis, we calculated features at time points spaced 20 ms apart, using time windows of 200 ms (90% overlap, resulting in 151 time windows). We used the SVM classifier to estimate the class membership probability[91] of each tested time instance for each of the odor identity classes of the three in-trial cue odors, which we refer to as reactivation strength (given ten total odor type classes, chance-level reactivation strength = 10%). Hence, for each maintenance trial, we obtained a 151 × 3 reactivation matrix X. Whereas the raw reactivations strengths were used in all analyses, for visualization of individual replay episodes, we *z*-scored normalized the reactivations strengths in X with respect to itself, for each of the three cue odors separately. All maintenance trials were used for the test set for this analysis.

We quantified “sequenceness,” or the degree to which neural representations followed a particular sequence, based on published methodology[49,53], described here in detail. First, transition from a neural representation of the first cue odor to that of the second cue odor ($S_1 \rightarrow S_2$), and from that of the second cue to the third cue ($S_2 \rightarrow S_3$) can be represented with the transition matrix T_f:

$$T_f = \begin{matrix} 0 & 1 & 0 \\ 0 & 0 & 1 \\ 0 & 0 & 0 \end{matrix}$$

The full-length original sequence ($S_1 \rightarrow S_2 \rightarrow S_3$) can then be represented with a transition matrix that is simply the second power of T_f: $T_{ff} = T_f^2$. We were also interested in the reverse sequence transitions ($S_3 \rightarrow S_2$, $S_2 \rightarrow S_1$), which can be represented by T_r as follows:

$$T_r = \begin{matrix} 0 & 0 & 0 \\ 1 & 0 & 0 \\ 0 & 1 & 0 \end{matrix}$$

The transition matrix T_{rr} for the full reverse sequence $S_3 \rightarrow S_2 \rightarrow S_1$ is again equal to T_r^2. Note that T_r and T_{rr} are simply the transpose of T_f and T_{ff}, respectively. As controls, we also computed sequenceness for the remaining four unique (non-sequential) permutations of length-3 transitions: $S_1 \rightarrow S_3 \rightarrow S_2$; $S_3 \rightarrow S_1 \rightarrow S_2$; $S_2 \rightarrow S_3 \rightarrow S_1$; and $S_2 \rightarrow S_1 \rightarrow S_3$.

The transition matrices were then applied to X:

$$X_f = X \times T_f$$

$$X_{ff} = X \times T_{ff}$$

If X contains forward sequences, then the decoding probability of S_1 at time t should correlate with the decoding probability of S_2 at $t + \Delta t$ and S_3 at $t + 2\Delta t$, where Δt is the time lag between reactivations. Hence, for a given Δt, we computed the cosine similarity between column *i* of X, column *i* of X_f, and column *i* of X_{ff}. These three values were then averaged to obtain the overall forward sequenceness. Reverse sequenceness was similarly calculated using T_r and T_{rr} in place of T_f and T_{ff}. To control for auto-correlations in the underlying signals at short intervals, the final results were reported as the difference between forward and reverse sequenceness at each evaluated time lag (30 time lags spanning 20 to 600 ms).

As the number of non-sequential length-3 sequences was not sufficient to assess significance by direct comparison, we generated a surrogate distribution of sequenceness differences. To control for differences in the number of trials across subjects, we chose, at each iteration (N = 1000), the minimum number of trials. We then calculated the true sequenceness difference, as well as the difference between two randomly-selected permuted sequences. Significance was determined independently at each evaluated time lag, if the observed sequenceness difference was outside the 99.83^{th} percentile of the surrogate distribution (corresponding to a two-tailed threshold of $p < 0.05$ after Bonferroni correction across the 30 time lags). The sequenceness difference at each time lag was reported after *z*-score normalizing the observed value with respect to the corresponding surrogate distribution.

Analysis during individual replay events—We followed published methodology to identify individual replay events[49]. Briefly, the onset of replay events was detected from each maintenance trial as time points at which a strong reactivation of the first cue odor was followed by strong reactivations of the remaining two cue odors in the sequence. For forward sequences, we time shifted the second and third columns of X by Δt and $2\Delta t$,

respectively, resulting in $X^{\Delta t}$, using the time lag Δt at which there was maximal evidence for sequenceness (namely, 200 ms). The second and third columns of $X^{\Delta t}$ were then element-wise multiplied with the second column of X_f and third column of X_{ff}, respectively. Finally, we summed over the three columns to obtain a vector R whose elements indicate the strength of sequenceness at each time point throughout an individual maintenance trial. To identify replay events, we thresholded R at the 95th percentile across its elements and across all trials.

To assess the impact of replay on subsequent memory on a trial-by-trial basis, we pooled all maintenance trials across subjects, and compared the prevalence of replay events (total number of replay events) in correct trials (on both the identity match and sequence position judgements) vs. all remaining trials. We then used a bootstrapping approach to demonstrate the robustness of this behavioral correlation. Across 10,000 bootstrapped subsets of trials, we computed a Pearson's correlation between the total number of replay events and the percentage of correct trials (each variable was *z*-score normalized with respect to itself prior to computing the correlation). To determine the stability of the correlation, this bootstrapping procedure was repeated 1,000 times, resulting in a distribution of 1,000 *r* values.

Closely following the procedure used for the phase separability analysis during the encoding period (see Theta phase coding of sequence position during encoding), we evaluated the separability of preferred theta phases of each cue odor reactivation during replay. Based on results of the sequenceness analysis, each 600-ms replay event ([−0.1, 0.5] s with respect to replay onset) was divided into three 200-ms epochs corresponding to each of the three cue odor reactivations ([−0.1, 0.1], [0.1, 0.3], [0.3, 0.5] s). From each epoch we constructed a theta phase distribution of reactivation-associated gamma power (*z*-score normalized with respect to the pre-encoding baseline), and then computed the weighted circular mean of the largest phase cluster, the angle of which was treated as the preferred theta phase of a cue odor reactivation. Phase separability between each unique pair of sequence positions was tested parametrically, using the same procedure as previously detailed. We additionally performed a surrogate-based test to demonstrate that the findings were not a mere result of sampling theta phases across three contiguous 200-ms windows. To do this, we repeated the analysis on 1,000 randomly-sampled time windows (of the same duration as replay events) throughout the included maintenance trials, where significance was reached if the observed test statistic was > 97.5th percentile of surrogate distribution (one-tailed). The observed *F*-statistic was reported after *z*-score normalizing with respect to the corresponding surrogate distribution.

Finally, theta-band phase synchrony between PCx and AH during replay events was quantified from the distribution of phase differences across the two regions using two different metrics. First, we employed the phase locking value (PLV)[56], which is quantified by the magnitude of the mean resultant vector of the cross-structural phase differences. To mitigate concerns of spurious phase locking resulting from volume conduction, which would be associated with a phase lag of zero[92], we eliminated time points with a phase lag < 5˚ prior to calculating the PLV. We further confirmed these results using the phase lag index[57] (PLI), which quantifies the asymmetry of the distribution of cross-structural

phase differences around zero, and is therefore unaffected by zero phase-lag volume conduction. To achieve a normal distribution, all PLV values were first transformed into Rayleigh's *z*-statistics, and PLI values were Fisher *z*-transformed. We similarly constructed a baseline distribution for each corresponding maintenance trial, in which we calculated the two synchrony metrics in 1,000 time-shifted windows (of the same duration as replay events). The observed synchrony metrics were then *z*-score normalized with respect to baseline distributions from the corresponding maintenance trial, allowing us to assess for changes in cross-structural phase synchrony during replay events relative to the baseline level throughout the entire maintenance epoch.

Supplementary Material

Refer to Web version on PubMed Central for supplementary material.

Acknowledgements:

This work was supported by NINDS Kirschstein-NRSA T32 postdoctoral grant (A.I.Y.), and NIDCD grant R01DC018075 (J.A.G.).

REFERENCES

1. Kesner RP, Gilbert PE, and Barua LA (2002). The role of the hippocampus in memory for the temporal order of a sequence of odors. Behav. Neurosci 116, 286–290. [PubMed: 11996313]
2. Fortin NJ, Agster KL, and Eichenbaum HB (2002). Critical role of the hippocampus in memory for sequences of events. Nat. Neurosci 5, 458–462. [PubMed: 11976705]
3. Pang R, Breugel F, Dickinson M, Riffell JA, and Fairhall A. (2018). History dependence in insect flight decisions during odor tracking. PLOS Computational Biology 14, e1005969. [PubMed: 29432454]
4. Vergassola M, Villermaux E, and Shraiman BI (2007). 'Infotaxis' as a strategy for searching without gradients. Nature 445, 406–409. [PubMed: 17251974]
5. Miles C, and Hodder K. (2005). Serial position effects in recognition memory for odors: a reexamination. Mem Cognit 33, 1303–1314.
6. Störmer VS, Alvarez GA, and Cavanagh P. (2014). Within-hemifield competition in early visual areas limits the ability to track multiple objects with attention. J. Neurosci 34, 11526–11533. [PubMed: 25164651]
7. Buschman TJ, Siegel M, Roy JE, and Miller EK (2011). Neural substrates of cognitive capacity limitations. PNAS 108, 11252–11255. [PubMed: 21690375]
8. Stettler DD, and Axel R. (2009). Representations of odor in the piriform cortex. Neuron 63, 854–864. [PubMed: 19778513]
9. Akam T, and Kullmann DM (2014). Oscillatory multiplexing of population codes for selective communication in the mammalian brain. Nature Reviews Neuroscience 15, 111–122. [PubMed: 24434912]
10. Buzsáki G, and Moser EI (2013). Memory, navigation and theta rhythm in the hippocampal-entorhinal system. Nature Neuroscience 16, 130–138. [PubMed: 23354386]
11. Wilson MA, Varela C, and Remondes M. (2015). Phase organization of networkcomputations. Current Opinion in Neurobiology 31, 250–253. [PubMed: 25679370]
12. Watrous AJ, Fell J, Ekstrom AD, and Axmacher N. (2015). More than spikes: common oscillatory mechanisms for content specific neural representations during perception and memory. Curr. Opin. Neurobiol 31, 33–39. [PubMed: 25129044]
13. Herman PA, Lundqvist M, and Lansner A. (2013). Nested theta to gamma oscillationsand precise spatiotemporal firing during memory retrieval in a simulated attractor network. Brain Res 1536, 68–87. [PubMed: 23939226]

14. Lundqvist M, Herman P, and Lansner A. (2011). Theta and gamma power increases and alpha/beta power decreases with memory load in an attractor network model. J Cogn Neurosci 23, 3008–3020. [PubMed: 21452933]
15. Mi Y, Katkov M, and Tsodyks M. (2017). Synaptic Correlates of Working Memory Capacity. Neuron 93, 323–330. [PubMed: 28041884]
16. Lisman JE, and Idiart MA (1995). Storage of 7 +/− 2 short-term memories in oscillatory subcycles. Science 267, 1512–1515. [PubMed: 7878473]
17. Jensen O, and Lisman JE (2005). Hippocampal sequence-encoding driven by a cortical multi-item working memory buffer. Trends Neurosci 28, 67–72. [PubMed: 15667928]
18. Axmacher N, Henseler MM, Jensen O, Weinreich I, Elger CE, and Fell J. (2010). Cross-frequency coupling supports multi-item working memory in the human hippocampus. Proc. Natl. Acad. Sci. U.S.A 107, 3228–3233. [PubMed: 20133762]
19. Bahramisharif A, Jensen O, Jacobs J, and Lisman J. (2018). Serial representation of items during working memory maintenance at letter-selective cortical sites. PLOS Biology 16, e2003805. [PubMed: 30110320]
20. Heusser AC, Poeppel D, Ezzyat Y, and Davachi L. (2016). Episodic sequence memory is supported by a theta-gamma phase code. Nat. Neurosci 19, 1374–1380. [PubMed: 27571010]
21. Siegel M, Warden MR, and Miller EK (2009). Phase-dependent neuronal coding of objects in short-term memory. Proc. Natl. Acad. Sci. U.S.A 106, 21341–21346. [PubMed: 19926847]
22. Buzsáki G, and Wang X-J (2012). Mechanisms of gamma oscillations. Annu. Rev. Neurosci 35, 203–225. [PubMed: 22443509]
23. Lundqvist M, Rose J, Herman P, Brincat SL, Buschman TJ, and Miller EK (2016). Gamma and Beta Bursts Underlie Working Memory. Neuron 90, 152–164. [PubMed: 26996084]
24. van Gerven MAJ, Maris E, Sperling M, Sharan A, Litt B, Anderson C, Baltuch G, and Jacobs J. (2013). Decoding the memorization of individual stimuli with direct human brain recordings. Neuroimage 70, 223–232. [PubMed: 23298746]
25. Jacobs J, and Kahana MJ (2009). Neural representations of individual stimuli in humans revealed by gamma-band electrocorticographic activity. J. Neurosci 29, 10203–10214. [PubMed: 19692595]
26. Brandon MP, Bogaard AR, Schultheiss NW, and Hasselmo ME (2013). Segregation of cortical head direction cell assemblies on alternating theta cycles. Nature Neuroscience 16, 739–748. [PubMed: 23603709]
27. Foster DJ, and Wilson MA (2007). Hippocampal theta sequences. Hippocampus 17, 1093–1099. [PubMed: 17663452]
28. Gupta AS, van der Meer MAA, Touretzky DS, and Redish AD (2012). Segmentation of spatial experience by hippocampal theta sequences. Nature Neuroscience 15, 1032–1039. [PubMed: 22706269]
29. Jezek K, Henriksen EJ, Treves A, Moser EI, and Moser M-B (2011). Theta-paced flickering between place-cell maps in the hippocampus. Nature 478, 246–249. [PubMed: 21964339]
30. Zhang X, Yan W, Wang W, Fan H, Hou R, Chen Y, Chen Z, Ge C, Duan S, Compte A, et al. (2019). Active information maintenance in working memory by a sensory cortex. eLife 8, e43191. [PubMed: 31232695]
31. Boeijinga PH, and Van Groen T. (1984). Inputs from the olfactory bulb and olfactory cortex to the entorhinal cortex in the cat. II. Physiological studies. Exp Brain Res 57, 40–48. [PubMed: 6519229]
32. Kay LM (2005). Theta oscillations and sensorimotor performance. PNAS 102, 3863–3868. [PubMed: 15738424]
33. Jiang H, Schuele S, Rosenow J, Zelano C, Parvizi J, Tao JX, Wu S, and Gottfried JA (2017). Theta Oscillations Rapidly Convey Odor-Specific Content in Human Piriform Cortex. Neuron 94, 207–219.e4. [PubMed: 28384472]
34. Zhou G, Olofsson JK, Koubeissi MZ, Menelaou G, Rosenow J, Schuele SU, Xu P, Voss JL, Lane G, and Zelano C. (2021). Human hippocampal connectivity is stronger in olfaction than other sensory systems. Progress in Neurobiology 201, 102027. [PubMed: 33640412]

35. Fell J, and Axmacher N. (2011). The role of phase synchronization in memory processes. Nature Reviews Neuroscience 12, 105–118. [PubMed: 21248789]
36. Sternberg S. (1966). High-speed scanning in human memory. Science 153, 652–654. [PubMed: 5939936]
37. Litaudon P, Garcia S, and Buonviso N. (2008). Strong coupling between pyramidal cell activity and network oscillations in the olfactory cortex. Neuroscience 156, 781–787. [PubMed: 18790020]
38. Eeckman FH, and Freeman WJ (1990). Correlations between unit firing and EEG in the rat olfactory system. Brain Research 528, 238–244. [PubMed: 2271924]
39. Kucewicz MT, Cimbalnik J, Matsumoto JY, Brinkmann BH, Bower MR, Vasoli V, Sulc V, Meyer F, Marsh WR, Stead SM, et al. (2014). High frequency oscillations are associated with cognitive processing in human recognition memory. Brain 137, 2231–2244. [PubMed: 24919972]
40. Dvorak D, and Fenton AA (2014). Toward a proper estimation of phase-amplitude coupling in neural oscillations. J Neurosci Methods 225, 42–56. [PubMed: 24447842]
41. van der Meij R, Kahana M, and Maris E. (2012). Phase-amplitude coupling in human electrocorticography is spatially distributed and phase diverse. J. Neurosci 32, 111–123. [PubMed: 22219274]
42. Watrous AJ, Deuker L, Fell J, and Axmacher N. (2015). Phase-amplitude coupling supports phase coding in human ECoG. Elife 4.
43. Canolty RT, Ganguly K, Kennerley SW, Cadieu CF, Koepsell K, Wallis JD, and Carmena JM (2010). Oscillatory phase coupling coordinates anatomically dispersed functional cell assemblies. PNAS 107, 17356–17361. [PubMed: 20855620]
44. Donoghue T, Haller M, Peterson EJ, Varma P, Sebastian P, Gao R, Noto T, Lara AH, Wallis JD, Knight RT, et al. (2020). Parameterizing neural power spectra into periodic and aperiodic components. Nature Neuroscience 23, 1655–1665. [PubMed: 33230329]
45. Raghavachari S, Kahana MJ, Rizzuto DS, Caplan JB, Kirschen MP, Bourgeois B, Madsen JR, and Lisman JE (2001). Gating of human theta oscillations by a working memory task. J. Neurosci 21, 3175–3183. [PubMed: 11312302]
46. Buzsáki G, and Tingley D. (2018). Space and Time: The Hippocampus as a Sequence Generator. Trends Cogn. Sci. (Regul. Ed.) 22, 853–869.
47. Eichenbaum H. (2017). On the Integration of Space, Time, and Memory. Neuron 95, 1007–1018. [PubMed: 28858612]
48. Chang C-C, and Lin C-J (2011). LIBSVM: A Library for Support Vector Machines. ACM Trans. Intell. Syst. Technol 2, 27:1–27:27.
49. Liu Y, Dolan RJ, Kurth-Nelson Z, and Behrens TEJ (2019). Human Replay Spontaneously Reorganizes Experience. Cell 178, 640–652.e14. [PubMed: 31280961]
50. Schuck NW, and Niv Y. (2019). Sequential replay of nonspatial task states in the human hippocampus. Science 364.
51. Eichenlaub J-B, Jarosiewicz B, Saab J, Franco B, Kelemen J, Halgren E, Hochberg LR, and Cash SS (2020). Replay of Learned Neural Firing Sequences during Rest in Human Motor Cortex. Cell Reports 31, 107581. [PubMed: 32375031]
52. Eldar E, Lièvre G, Dayan P, and Dolan RJ (2020). The roles of online and offline replay in planning. eLife 9, e56911. [PubMed: 32553110]
53. Kurth-Nelson Z, Economides M, Dolan RJ, and Dayan P. (2016). Fast Sequences of Non-spatial State Representations in Humans. Neuron 91, 194–204. [PubMed: 27321922]
54. Kamiński J, Brzezicka A, Mamelak AN, and Rutishauser U. (2020). Combined Phase-Rate Coding by Persistently Active Neurons as a Mechanism for Maintaining Multiple Items in Working Memory in Humans. Neuron
55. Fuentemilla L, Penny WD, Cashdollar N, Bunzeck N, and Düzel E. (2010). Theta-Coupled Periodic Replay in Working Memory. Curr Biol 20, 606–612. [PubMed: 20303266]
56. Lachaux J-P, Rodriguez E, Martinerie J, and Varela FJ (1999). Measuring phase synchrony in brain signals. Human Brain Mapping 8, 194–208. [PubMed: 10619414]

57. Stam CJ, Nolte G, and Daffertshofer A. (2007). Phase lag index: assessment of functional connectivity from multi channel EEG and MEG with diminished bias from common sources. Hum Brain Mapp 28, 1178–1193. [PubMed: 17266107]
58. Kay LM, Beshel J, Brea J, Martin C, Rojas-Líbano D, and Kopell N. (2009). Olfactory oscillations: the what, how and what for. Trends Neurosci 32, 207–214. [PubMed: 19243843]
59. Johnson EL, Adams JN, Solbakk A-K, Endestad T, Larsson PG, Ivanovic J, Meling TR, Lin JJ, and Knight RT (2018). Dynamic frontotemporal systems process space and time in working memory. PLOS Biology 16, e2004274. [PubMed: 29601574]
60. Vaz AP, Yaffe RB, Wittig JH, Inati SK, and Zaghloul KA (2017). Dual origins of measured phase-amplitude coupling reveal distinct neural mechanisms underlying episodic memory in the human cortex. Neuroimage 148, 148–159. [PubMed: 28065849]
61. Mormann F, Fell J, Axmacher N, Weber B, Lehnertz K, Elger CE, and Fernández G. (2005). Phase/amplitude reset and theta-gamma interaction in the human medial temporal lobe during a continuous word recognition memory task. Hippocampus 15, 890–900. [PubMed: 16114010]
62. Lega B, Burke J, Jacobs J, and Kahana MJ (2016). Slow-Theta-to-Gamma Phase-Amplitude Coupling in Human Hippocampus Supports the Formation of New Episodic Memories. Cereb. Cortex 26, 268–278. [PubMed: 25316340]
63. Maris E, van Vugt M, and Kahana M. (2011). Spatially distributed patterns of oscillatory coupling between high-frequency amplitudes and low-frequency phases in human iEEG. Neuroimage 54, 836–850. [PubMed: 20851192]
64. Leszczyński M, Fell J, and Axmacher N. (2015). Rhythmic Working Memory Activation in the Human Hippocampus. Cell Rep 13, 1272–1282. [PubMed: 26527004]
65. Chaieb L, Leszczynski M, Axmacher N, Höhne M, Elger CE, and Fell J. (2015). Theta-gamma phase-phase coupling during working memory maintenance in the human hippocampus. Cogn Neurosci 6, 149–157. [PubMed: 26101947]
66. Emrich SM, Riggall AC, Larocque JJ, and Postle BR (2013). Distributed patterns of activity in sensory cortex reflect the precision of multiple items maintained in visual short-term memory. J. Neurosci 33, 6516–6523. [PubMed: 23575849]
67. Ester EF, Anderson DE, Serences JT, and Awh E. (2013). A neural measure of precision in visual working memory. J Cogn Neurosci 25, 754–761. [PubMed: 23469889]
68. D'Esposito M, and Postle BR (2015). The Cognitive Neuroscience of Working Memory. Annu Rev Psychol 66, 115–142. [PubMed: 25251486]
69. Colgin LL (2016). Rhythms of the hippocampal network. Nature Reviews Neuroscience 17, 239–249. [PubMed: 26961163]
70. Euston DR, Gruber AJ, and McNaughton BL (2012). The Role of Medial Prefrontal Cortex in Memory and Decision Making. Neuron 76, 1057–1070. [PubMed: 23259943]
71. Ji D, and Wilson MA (2007). Coordinated memory replay in the visual cortex and hippocampus during sleep. Nature Neuroscience 10, 100–107. [PubMed: 17173043]
72. Rothschild G, Eban E, and Frank LM (2017). A cortical-hippocampal-cortical loop of information processing during memory consolidation. Nat. Neurosci 20, 251–259. [PubMed: 27941790]
73. Ólafsdóttir HF, Carpenter F, and Barry C. (2016). Coordinated grid and place cell replay during rest. Nat. Neurosci 19, 792–794. [PubMed: 27089021]
74. Benchenane K, Peyrache A, Khamassi M, Tierney PL, Gioanni Y, Battaglia FP, and Wiener SI (2010). Coherent theta oscillations and reorganization of spike timing in the hippocampal-prefrontal network upon learning. Neuron 66, 921–936. [PubMed: 20620877]
75. Jones MW, and Wilson MA (2005). Theta rhythms coordinate hippocampal-prefrontal interactions in a spatial memory task. PLoS Biol 3, e402. [PubMed: 16279838]
76. Skaggs WE, and McNaughton BL (1996). Replay of neuronal firing sequences in rat hippocampus during sleep following spatial experience. Science 271, 1870–1873. [PubMed: 8596957]
77. Wikenheiser AM, and Redish AD (2015). Hippocampal theta sequences reflect current goals. Nat. Neurosci 18, 289–294. [PubMed: 25559082]
78. Pezzulo G, Donnarumma F, Maisto D, and Stoianov I. (2019). Planning at decision time and in the background during spatial navigation. Current Opinion in Behavioral Sciences 29, 69–76.

79. Strange BA, Witter MP, Lein ES, and Moser EI (2014). Functional organization of the hippocampal longitudinal axis. Nature Reviews Neuroscience 15, 655–669. [PubMed: 25234264]
80. Goyal A, Miller J, Qasim SE, Watrous AJ, Zhang H, Stein JM, Inman CS, Gross RE, Willie JT, Lega B, et al. (2020). Functionally distinct high and low theta oscillations in the human hippocampus. Nature Communications 11, 2469.
81. Seubert J, Freiherr J, Djordjevic J, and Lundström JN (2013). Statistical localization of human olfactory cortex. Neuroimage 66, 333–342. [PubMed: 23103688]
82. Kesner RP, Hunsaker MR, and Ziegler W. (2011). The role of the dorsal and ventral hippocampus in olfactory working memory. Neurobiol Learn Mem 96, 361–366. [PubMed: 21742047]
83. Smith SM, Jenkinson M, Woolrich MW, Beckmann CF, Behrens TEJ, Johansen-Berg H, Bannister PR, De Luca M, Drobnjak I, Flitney DE, et al. (2004). Advances in functional and structural MR image analysis and implementation as FSL. Neuroimage 23 Suppl 1, S208–219. [PubMed: 15501092]
84. Brainard DH (1997). The Psychophysics Toolbox. Spat Vis 10, 433–436. [PubMed: 9176952]
85. Delorme A, and Makeig S. (2004). EEGLAB: an open source toolbox for analysis of single-trial EEG dynamics including independent component analysis. J. Neurosci. Methods 134, 9–21. [PubMed: 15102499]
86. Li G, Jiang S, Paraskevopoulou SE, Wang M, Xu Y, Wu Z, Chen L, Zhang D, and Schalk G. (2018). Optimal referencing for stereo-electroencephalographic (SEEG) recordings. NeuroImage 183, 327–335. [PubMed: 30121338]
87. Arnulfo G, Hirvonen J, Nobili L, Palva S, and Palva JM (2015). Phase and amplitude correlations in resting-state activity in human stereotactical EEG recordings. Neuroimage 112, 114–127. [PubMed: 25721426]
88. Miller KJ, Sorensen LB, Ojemann JG, and den Nijs M. (2009). Power-law scaling in the brain surface electric potential. PLoS Comput. Biol 5, e1000609. [PubMed: 20019800]
89. Maris E, and Oostenveld R. (2007). Nonparametric statistical testing of EEG- and MEG-data. J. Neurosci. Methods 164, 177–190. [PubMed: 17517438]
90. Berens P. (2009). CircStat: A MATLAB Toolbox for Circular Statistics. Journal of Statistical Software 31, 1–21.
91. Wu T-F, Lin C-J, and Weng RC (2004). Probability Estimates for Multi-class Classification by Pairwise Coupling. Journal of Machine Learning Research 5, 975–1005.
92. Aydore S, Pantazis D, and Leahy RM (2013). A note on the phase locking value and its properties. Neuroimage 74, 231–244. [PubMed: 23435210]

Yang *et. al* investigate neural oscillations during the encoding and maintenance of a sequence of distinct odors in working memory. Analogous to rodent theta sequences, replay of experienced odor sequences in the human olfactory (piriform) cortex is time-compressed, forward-directed, and coincides with the hippocampal theta rhythm.

- Nested oscillations underlie working memory representations of multi-odor sequences
- Theta oscillations disambiguate sequence odors across multiple timescales
- During memory maintenance, sequences are replayed across successive theta cycles
- Online replay in humans predicts subsequent recall performance

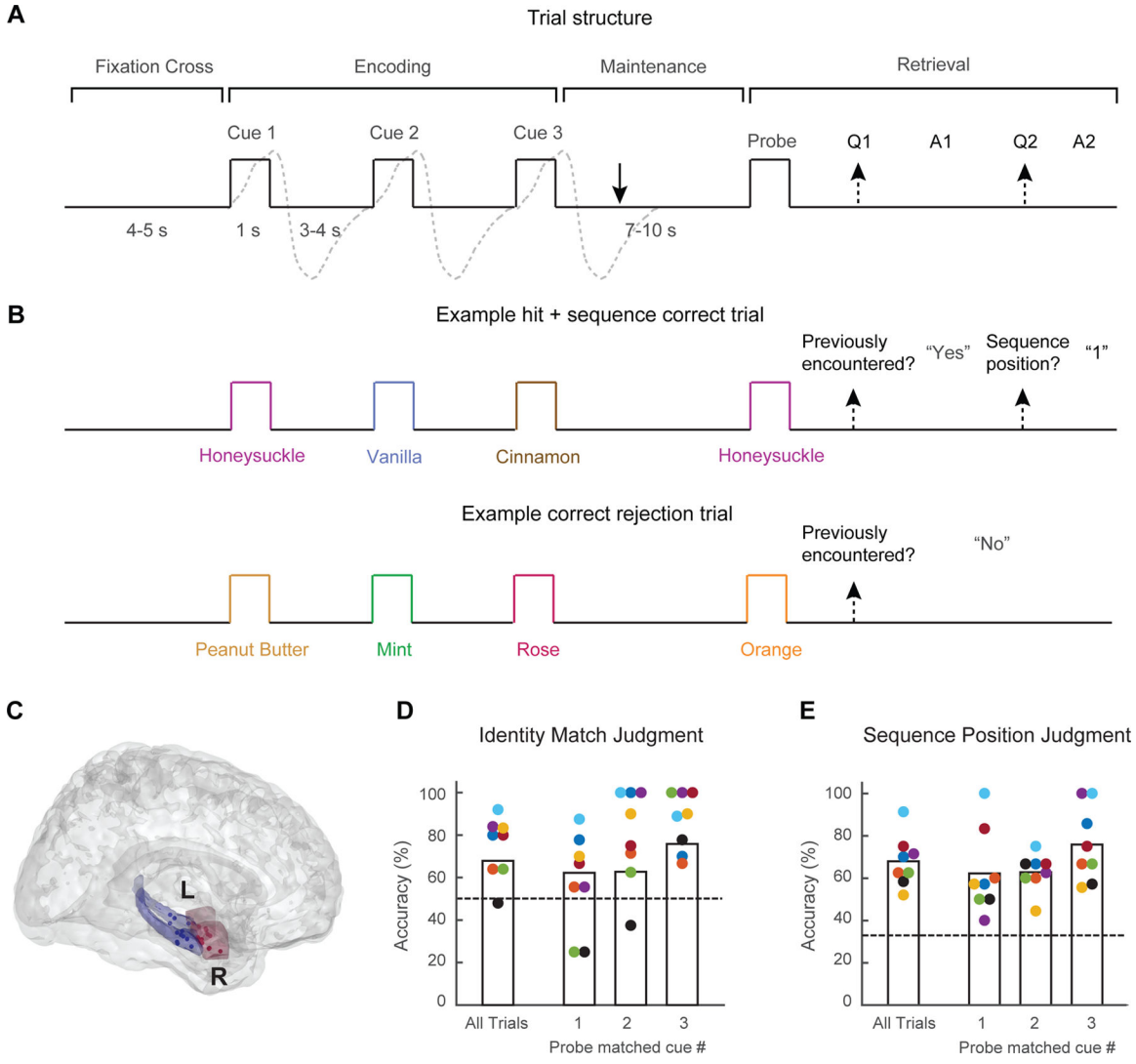

Figure 1. Experimental approach.

(A) Task structure. Trials began with a fixation cross, after which subjects were sequentially presented with three distinct cue odors (encoding). Following a delay period (maintenance), subjects performed up to two judgments on a final probe odor (retrieval): an identity match judgment, and, as appropriate, a sequence position judgment. For encoding and retrieval, analyzed epochs began at sniff onset (illustrated with gray dashed lines). Analyzed maintenance epochs began one second after the end of the inhalation in response to Cue 3 (solid arrow). Baseline epochs were extracted from the pre-encoding fixation cross period. **(B)** Example trials of correct responses (top panel) to the identity match judgment (i.e., hit) and sequence position judgment, or correct rejection (bottom panel) of a novel probe odor. **(C)** Electrode positions across all subjects. Recordings obtained from PCx in seven subjects, AH in six subjects, with simultaneous recordings from both regions in five subjects. Red, PCx; blue, AH. See also Figure S1, Table S1.

(**D, E**) Behavioral performance on (**D**) the identity match judgment or (**E**) the sequence position judgment for all trials, as well as for the subset of trials in which the probe odor

matched the first, second, or third cue odors. Colors indicate individual subjects; dashed lines indicate chance-level accuracy.

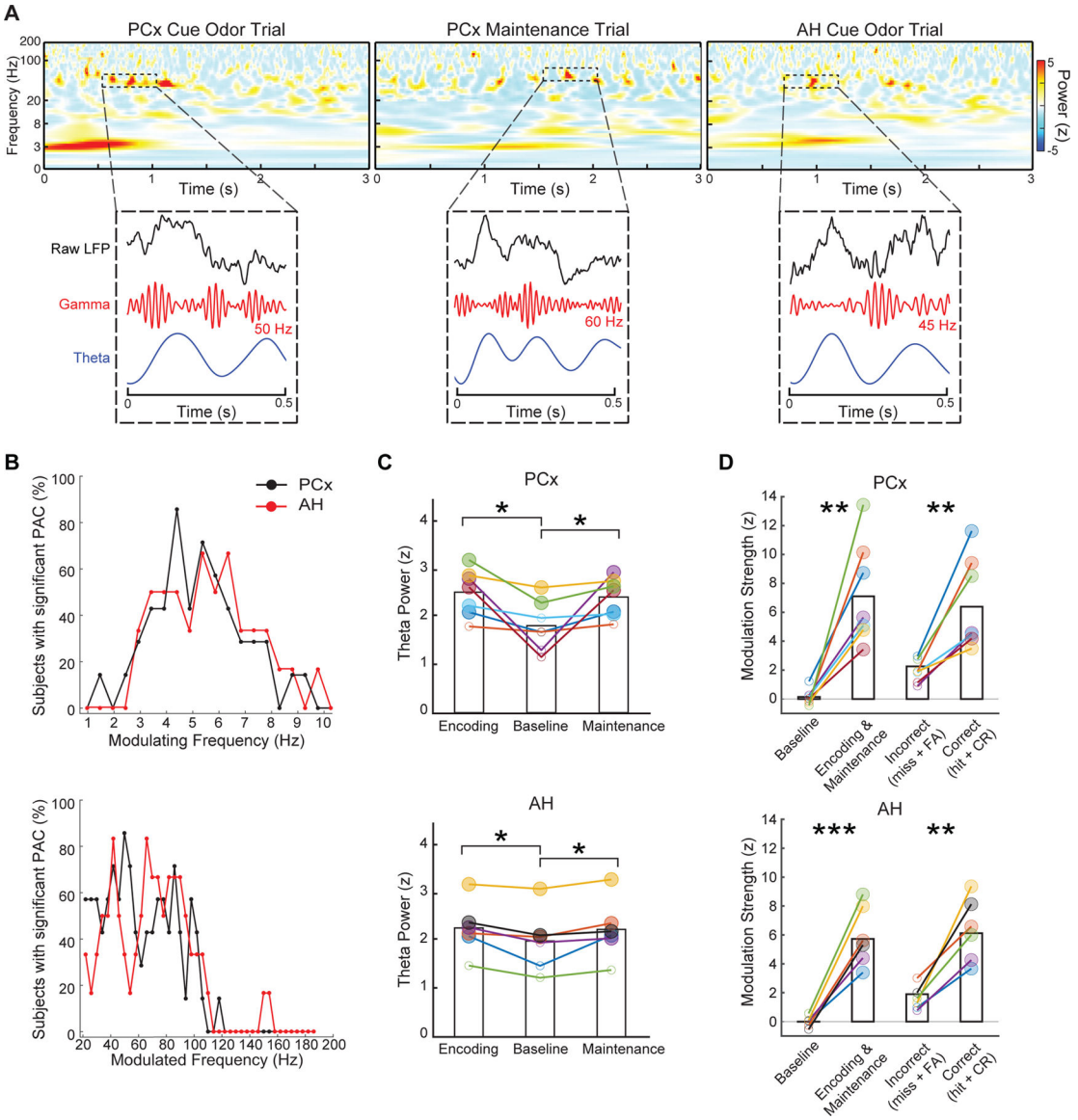

Figure 2. Coupled theta and gamma oscillations.

(A) Single trial examples (from different subjects) show multiple, brief bursts of high-frequency activity throughout encoding and maintenance, concurrent with theta oscillations. For each trial, we show the raw LFP, high frequency filtered signal, and theta filtered signal (relatively scaled for visualization) centered around one of the bursts. Note the diversity in the center frequencies of bursts, both within and across subjects. Across all subjects, burst duration was 107 ± 18 ms (mean ± s.e.m.) in PCx, and 98 ± 14 ms in AH (see Methods). **(B)** PAC during encoding and maintenance was quantified across a wide range of candidate modulating frequencies (top panel) and modulated frequencies (bottom panel). Across evaluated frequencies, we show the percentage of subjects demonstrating significant modulation strength (surrogate test, corrected across modulated sub-bands, $p < 0.025$), separately for PCx and AH. See also Figure S2.

(C) In both regions of interest, theta power during encoding and maintenance were individually greater vs. baseline (paired-sample *t*-test, $*p < 0.05$). Larger solid circles indicate supra-threshold theta power; smaller empty circles indicate sub-threshold power (see Methods). See also Figure S3.

(D) Modulation strengths of theta phase-coupled gamma bursts were increased during encoding and maintenance vs. baseline, which was further stratified for identity-match correct (hit + correct rejection [CR]) vs. incorrect (miss + false alarm [FA]) trials. Larger solid circles indicate significant modulation strength (corrected, $p < 0.025$). $**p < 0.01$; $***p < 0.001$. See also Figure S3D.

In (**C**-**D**), colors indicate individual subjects.

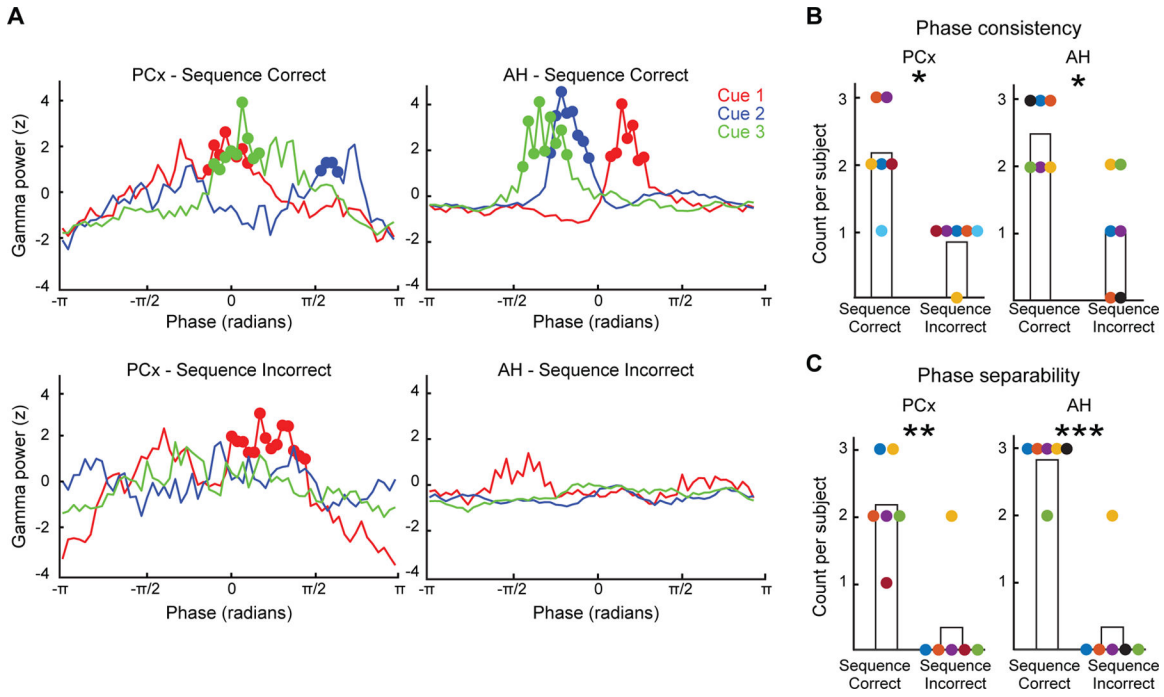

Figure 3. Encoding the "when" of odor sequences.

(**A-B**) Cross-trial consistency of theta phase preference for each sequence position. (**A**) For each sequence position, we show single-subject trial-averaged theta phase distributions of cue odor-induced gamma power (PCx and AH data from different subjects). In both regions of interest, cue odors in each position induced gamma within specific phase ranges of theta during successful sequence encoding (solid circles; cluster-corrected $p < 0.025$). In contrast, in sequence-incorrect trials, odor-induced gamma did not demonstrate a consistent cross-trial theta phase preference (in PCx example subject, only Cue 1 was associated with a significant phase cluster). (**B**) At the group level, the number of sequence positions with significant phase clusters for each subject was greater during successful vs. unsuccessful sequence memory formation (paired-sample *t*-test, $*p < 0.05$).

(**C**) Separability of theta phase preference between sequence positions. The preferred theta phases of single trial responses to cue odors were compared between each unique pair of sequence positions (position 1 vs. 2, 2 vs. 3, 1 vs. 3). The number of significant pairwise phase comparisons per subject was greater during sequence-correct vs. incorrect trials ($**p < 0.01$, $***p < 0.001$).

In (**B, C**), colors indicate individual subjects.

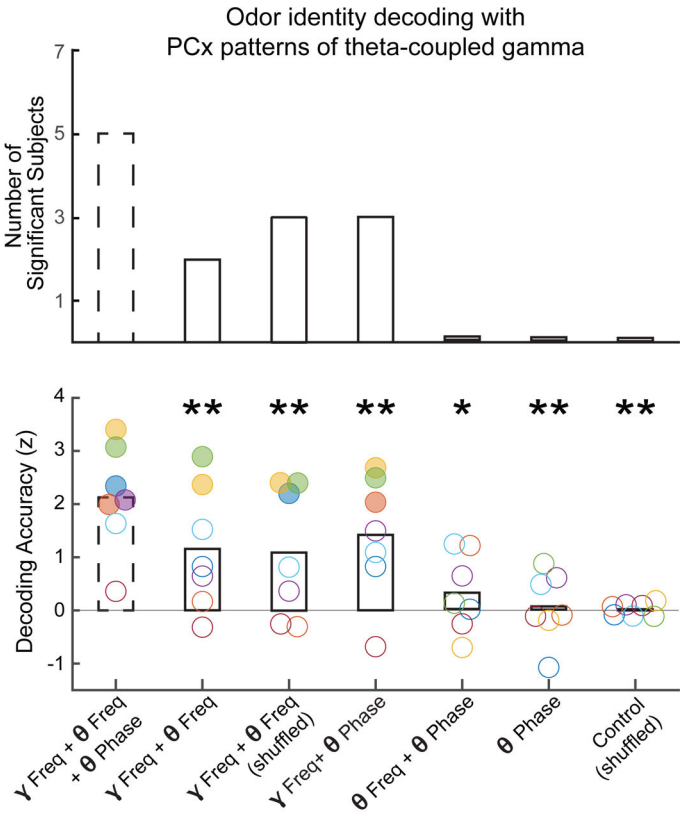

Feature spaces depicting theta-coupled gamma

		Axis i (γ Freq)	Axis ii (θ Freq)	Axis iii (θ Phase)
1	γ Freq + θ Freq + θ Phase	✓	✓	✓
2	γ Freq + θ Freq	✓	✓	×
3	γ Freq + θ Phase	✓	×	✓
4	θ Freq + θ Phase	×	✓	✓
5	θ Phase	×	×	✓
6	Control	×	×	×

Figure 4. Encoding the "what" of odor sequences.

Odor identity was decoded from single-trial PCx responses to cue odors, in which the pattern of stimulus-induced theta-coupled gamma was depicted across three axes: i. gamma frequency, ii. theta frequency, and iii. theta phase. To validate this feature space (1 in the table), classification was also performed with reduced-dimensionality feature spaces, in which the pattern of theta-coupled gamma was only depicted across the following axes: (2) gamma frequency + theta frequency; (3) gamma frequency + theta phase; (4) theta frequency + theta phase; and (5) theta phase only. Finally, classification was also performed with a control feature space in which information along all three axes were disrupted (6). For each feature space, we show the number of subjects with significant decoding (surrogate test, $p < 0.05$; top panel), as well as subject-level decoding accuracies, normalized with respect to feature space-specific surrogate distributions (middle panel; colors indicate individual subjects; solid circles indicate significant decoding). Classification of odor identity with

the full three-dimensional feature space (dashed bars) was significant in five (out of seven subjects), and was more accurate than for the reduced-dimensionality feature spaces (paired-sample *t*-test, $*p < 0.05$, $**p < 0.01$). Raw decoding accuracies were as follows (chance level accuracy = 10%): (1) 13.9 ± 0.4%; (2)12.5 ± 0.4% or 12.6 ± 0.4% (shuffled), (3) 13.0 ± 0.3%, (4) 10.9 ± 0.2%, (5) 10.5 ± 0.2%, (6) 10.5 ± 0.1%. In the table, ✓ indicates that the distribution of gamma power across a specific axis was preserved; × indicates that information across a specific axis was discarded, by either taking the average gamma power or by shuffling their values across the axis being removed (see Methods). See also Figure S4A-E for visualizations of each feature space.

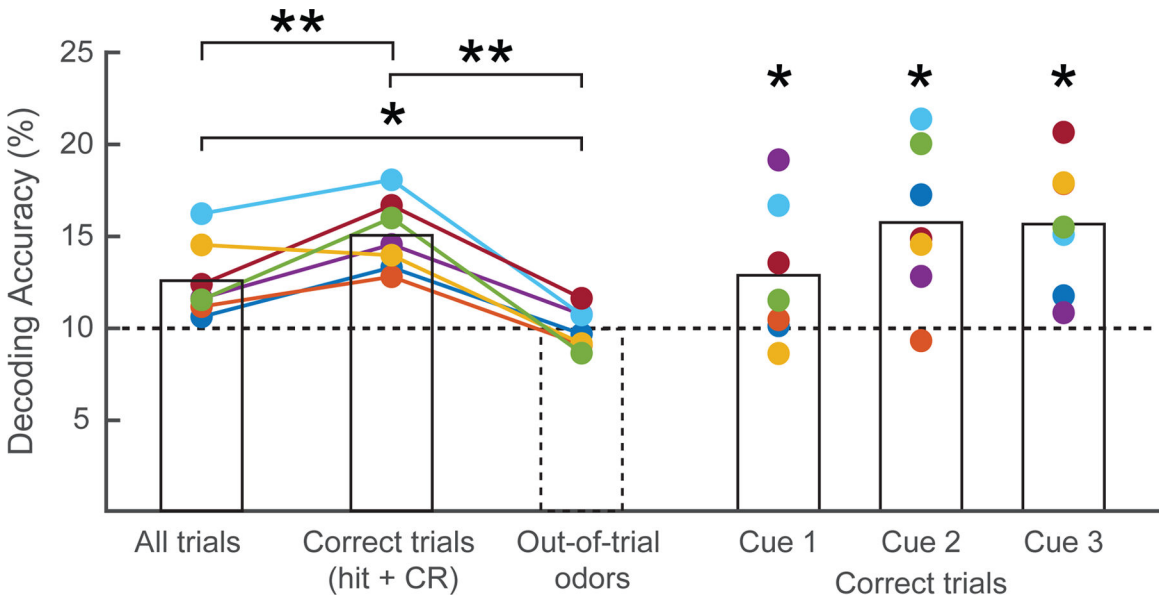

Figure 5. Reactivation of individual cue odors during maintenance.

In PCx, working memory content during the delay period was decoded using a classifier trained on cue odor-induced patterns of theta-coupled gamma. When including all maintenance trials, classification accuracy for the three in-trial cue odors was higher than for the seven out-of-trial odors (paired-sample *t*-test, $*p < 0.05$). Model performance further improved when classification was limited to maintenance trials preceding a correct identity match judgment (hit or correct rejection [CR]; $**p < 0.01$). For the set of identity correct trials, decoding accuracies for cue odors presented in each of the three sequence positions were each higher vs. out-of-trial odors. Horizontal dashed line indicates chance-level accuracy; colors indicate individual subjects.

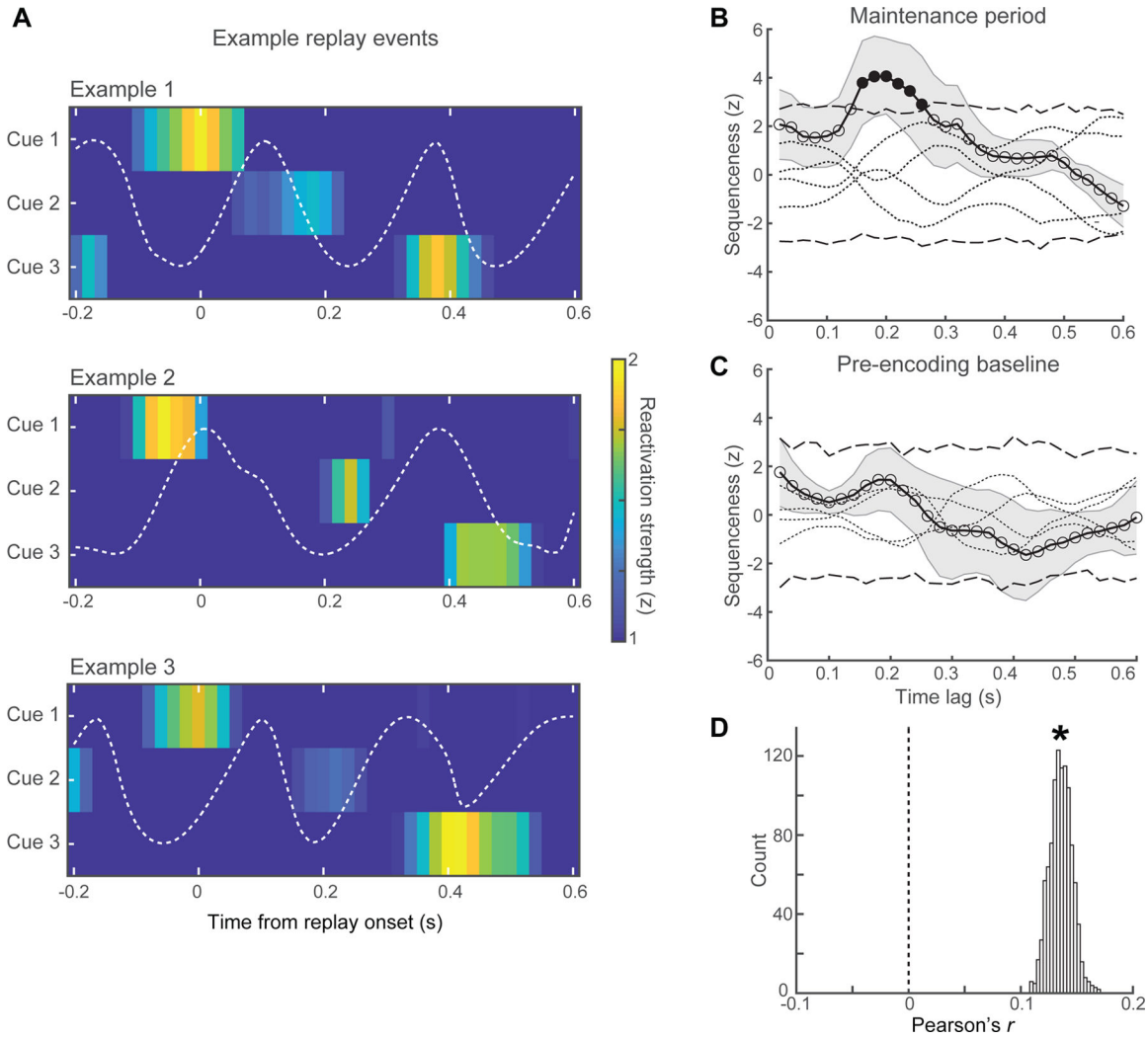

Figure 6. Theta-timescale replay of odor sequences during maintenance.

(A) Memory replay examples (from different subjects) in PCx during working memory maintenance. Sequential reactivation of the three cue odors consistently emerged earliest for cue 1, followed by cue 2, and terminating with cue 3, whereby each reactivation took place in separate theta cycles. Theta-filtered signals overlaid in white.

(B, C) Statistical evidence for replay. **(B)** During maintenance, there was evidence for forward sequenceness at an inter-reactivation time lag of 160–260 ms (solid black circles; corrected across time lags, $p < 0.05$). **(C)** There was no evidence of sequenceness in the pre-encoding baseline period. Sequenceness is shown for the four permuted (non-sequential) length-3 sequences (dotted lines; see Methods); dashed lines indicate 99.83% CI of surrogate distribution constructed from these permuted sequences; shading indicates s.e.m. across subjects.

(D) Pooling all maintenance trials across subjects, replay events were more common prior to a correct (vs. incorrect) response on the identity match and sequence position judgments (see Results). The robustness of this finding was demonstrated with a bootstrapping approach, in which the prevalence of replay events was correlated with the percentage of correct trials.

Across 1,000 repetitions of this bootstrapping procedure, the distribution of Pearson's r showed a stable positive correlation (*95% CI of r [0.12, 0.15]).

KEY RESOURCES TABLE

REAGENT or RESOURCE	SOURCE	IDENTIFIER
Experimental Models: Organisms/Strains		
Human Epilepsy Patients	Northwestern Memorial Hospital, Hospital of the University of Pennsylvania	n/a
Deposited Data		
Human Intracranial Data		https://www.ieeg.org/
Software and Algorithms		
MATLAB	MathWorks	https://www.mathworks.com/
PsychToolbox	[84]	http://psychtoolbox.org/
EEGLAB	[85]	https://sccn.ucsd.edu/eeglab/index.php
Fitting Oscillations & One Over F (FOOOF)	[44]	https://github.com/fooof-tools/fooof
CircStat	[90]	http://bethgelab.org/software/circstat/
LibSVM	[48]	https://www.csie.ntu.edu.tw/~cjlin/libsvm/
Sequenceness	[49]	https://github.com/YunzheLiu/FactorizedReplay